nature cell biology

A secreted peptide acts on BIN2-mediated phosphorylation of ARFs to potentiate auxin response during lateral root development

Hyunwoo Cho[1,7], Hojin Ryu[1,7], Sangchul Rho[2], Kristine Hill[3,4], Stephanie Smith[3], Dominique Audenaert[5,6], Joonghyuk Park[1], Soeun Han[1], Tom Beeckman[5,6], Malcolm J. Bennett[3,4], Daehee Hwang[2], Ive De Smet[3,5,6] and Ildoo Hwang[1,8]

The phytohormone auxin is a key developmental signal in plants. So far, only auxin perception has been described to trigger the release of transcription factors termed AUXIN RESPONSE FACTORs (ARFs) from their AUXIN/INDOLE-3-ACETIC ACID (AUX/IAA) repressor proteins. Here, we show that phosphorylation of ARF7 and ARF19 by BRASSINOSTEROID-INSENSITIVE2 (BIN2) can also potentiate auxin signalling output during lateral root organogenesis. BIN2-mediated phosphorylation of ARF7 and ARF19 suppresses their interaction with AUX/IAAs, and subsequently enhances the transcriptional activity to their target genes *LATERAL ORGAN BOUNDARIES-DOMAIN16* (*LBD16*) and *LBD29*. In this context, BIN2 is under the control of the TRACHEARY ELEMENT DIFFERENTIATION INHIBITORY FACTOR (TDIF)–TDIF RECEPTOR (TDR) module. TDIF-initiated TDR signalling directly acts on BIN2-mediated ARF phosphorylation, leading to the regulation of auxin signalling during lateral root development. In summary, this study delineates a TDIF–TDR–BIN2 signalling cascade that controls regulation of ARF and AUX/IAA interaction independent of auxin perception during lateral root development.

Spatial and temporal regulation of auxin signalling is essential for diverse developmental processes in plants[1], and the nuclear auxin response mechanism has been well characterized[2,3]. In brief, auxin maxima formation through its graded distribution promotes the interaction between its co-receptors, TRANSPORT INHIBITOR1 (TIR1) or AUXIN-SIGNALLING F-BOX PROTEIN (AFB) F-box proteins and AUX/IAA transcriptional repressors, which triggers degradation of AUX/IAAs by E3 ubiquitin-ligase $SCF^{TIR1/AFBs}$ complexes[4]. At low auxin levels, AUX/IAA repressors are stable and interact with ARF transcription factors, and recruit co-repressor complexes leading to suppression of auxin-responsive genes[1,5]. At higher auxin levels, degradation of AUX/IAAs allows free ARFs to initiate transcription of auxin-responsive genes[2,3]. In *Arabidopsis*, interactions between 6 TIR1/AFB auxin receptors, 23 ARF proteins, and 29 AUX/IAA repressors are associated with diverse auxin responses during plant growth and development[1]. Distinct expression patterns of these central components, and remarkable differences in binding affinities between TIR1/AFBs and AUX/IAAs, could potentially result in a broad range of auxin signalling outputs[6]. Whereas the molecular basis of auxin perception and subsequent proteolysis of AUX/IAAs has been elucidated, the regulatory mechanism underlying how ARFs determine auxin signalling output and dissociate from the repressor complex is still unclear.

One important, well-characterized developmental process that is dependent on the tight regulation of ARFs and AUX/IAAs is lateral root (LR) initiation, patterning and emergence[7–9]. The auxin response module composed of ARF7 and ARF19 along with the target genes *LBD16* and *LBD29* controls LR organogenesis through auxin-dependent degradation of AUX/IAAs, such as SOLITARY ROOT (SLR)/IAA14 and MASSUGU 2 (MSG2)/IAA19 (refs 10,11).

GLYCOGEN SYNTHASE KINASE3 (GSK3) is a key regulator of diverse developmental processes in animals[12]. In *Arabidopsis*, distinct expression patterns of *GSK3*-like genes have been observed in various developing organs[13,14]. However, molecular links connecting these

[1]Department of Life Sciences, Pohang University of Science and Technology, Pohang 790-784, Korea. [2]School of Interdisciplinary Bioscience and Bioengineering, Pohang University of Science and Technology, Pohang 790-784, Korea. [3]Division of Plant and Crop Sciences, School of Biosciences University of Nottingham, Sutton Bonington Campus, Loughborough LE12 5RD, UK. [4]Centre for Plant Integrative Biology, University of Nottingham, Sutton Bonington Campus, Loughborough LE12 5RD, UK. [5]Integrative Plant Biology Division, Department of Plant Systems Biology, VIB, Technologiepark 927, Ghent 9052, Belgium. [6]Department of Plant Biotechnology and Bioinformatics, Ghent University, Technologiepark 927, Ghent 9052, Belgium. [7]These authors contributed equally to this work.
[8]Correspondence should be addressed to I.H. (e-mail: ihwang@postech.ac.kr)

Received 19 April 2013; accepted 11 November 2013; published online 22 December 2013; DOI: 10.1038/ncb2893

genes to development are largely unknown. The plant GSK3 BIN2 (also known as ULTRACURVATA1, UCU1, and DWARF12, DWF12) is a critical regulator in brassinosteroid (BR) signal transduction and stomata development[15,16]. BIN2 kinase targets YODA (YDA) and SPEECHLESS (SPCH) in stomata development[15,17], and negatively regulates BR signalling by phosphorylation-dependent inactivation of two BR-related key transcriptional regulators, *bri1* EMS SUPPRESSOR1 (BES1) and its homologue BRASSINAZOLE RESISTANT1 (BZR1; refs 18–20). The negative action of BIN2 in BR signalling is directly relieved by a phosphatase BSU1 (ref. 21). In addition to its action in BR signalling, BIN2 has been implicated in the regulation of auxin signalling[22,23]. A gain-of-function allele of BIN2, *ucu1*, showed auxin hypersensitivity in root elongation[22], and BIN2 seemed to attenuate DNA-binding affinity of ARF2, a repressor of auxin signalling[23]. However, it is largely unknown how BIN2 action is integrated into auxin signalling pathways during plant growth and development.

Here, we show that the TDIF–TDR–BIN2 signalling module directly regulates auxin signalling output during LR organogenesis by controlling the transcriptional activity of ARF7 and ARF19.

RESULTS

BIN2 positively regulates LR development

As BIN2 has been implicated in the regulation of auxin signalling[22,23], we investigated its role in auxin-mediated LR development. We examined the LR phenotype of gain-of-function *BIN2* mutants *dwf12-1D-gof* and *bin2-1-gof*, which exhibited a brassinosteroid (BR)-insensitive short root[24,25], and we observed an increased LR density compared with wild-type plants (Fig. 1a–c). In contrast, loss-of-function *BIN2* mutants *bin2-3-lof* (ref. 13) and *bin2-3 bil1 bil2* (ref. 26) exhibited a reduced LR density compared with wild-type plants (Fig. 1a,b). To eliminate the possibility that the LR phenotypes of *dwf12-1D-gof* and *bin2-1-gof* are due to their relatively short root length, the BR-insensitive mutant *bri1-116* was also examined. Indeed, although *bri1-116* exhibited a shorter root phenotype, this was not associated with increased LR density compared with wild-type plants (Fig. 1d). Furthermore, the *bin2-3 bil1 bil2* mutant phenotype was recapitulated in seedlings treated with bikinin, a GSK3-specific inhibitor[27] (Fig. 1a,b).

The involvement of BIN2 in root branching was further supported by examination of the *pBIN2–GUS* reporter line[18]. *BIN2* expression was detected in xylem pole pericycle cells, epidermal cells and cortex in the basal meristem, but restricted to the vasculature in the elongation zone (Fig. 1e and Supplementary Fig. 1a). During LR development, *BIN2* expression was observed in LR initiation sites and in the basal part of the dome-shaped LR primordium (Fig. 1e and Supplementary Fig. 1a).

To evaluate the physiological basis of the BR signalling pathway in LR development, we examined the role of the BR receptor BRI1, the BR biosynthesis enzyme DWARF4 (DWF4), and the downstream components BRI1 SUPPRESSOR 1 (BSU1), BES1 and BZR1. Interestingly, *DWF4*- (ref. 28) and *BRI1*- (ref. 29) overexpressing plants exhibited a higher density of LR primordia than wild-type plants, whereas *BSU1*-overexpressing[30] and gain-of function *bes1-D* (ref. 20) and *bzr1-1D* (ref. 19) plants did not (Fig. 2a). Furthermore, BR treatment further increased LR development in *bin2-1-gof*, but not in the *bri1-116* mutant, and *BIN2* overexpression increased LR development in the loss-of-function *bri1-5* mutant (Fig. 2b–d). These results indicate that BIN2 positively regulates LR initiation, and that BR action in LR development is bifurcated upstream of BSU1, an inhibitor of BIN2.

BIN2 enhances auxin response during LR development through ARF7 and ARF19

The *BIN2* expression patterns during LR development and in the vasculature overlapped with several well-known auxin-related transcriptional regulators for LR development, including *ARF5*, *ARF7*, *ARF19, IAA1, IAA3, IAA12, IAA14, IAA18* and *IAA19* (Supplementary Fig. 1b,c)[10,11,31,32]. Thus, we investigated whether BIN2 is connected to auxin signalling during LR development. First, we found that *dwf12-1D-gof* was hypersensitive to auxin with respect to primary root growth, whereas *bin2-3-lof* was less sensitive compared with wild-type plants (Fig. 3a). Next, after auxin depletion by NPA treatment, the auxin-responsive reporter *pDR5–GUS* was more rapidly and strongly activated by auxin in *bin2-1-gof* than in wild-type plants, particularly in the pericycle (Fig. 3b and Supplementary Fig. 2a). Moreover, expression of *LBD16* and *LBD29*, which are marker genes for LR initiation that function directly downstream of ARF7 and ARF19, was higher in *bin2-1-gof* and lower in *bri1-116* compared with wild-type plants (Supplementary Fig. 2b). To further confirm the *in planta* molecular action of BIN2 during auxin-mediated LR development, auxin sensitivity of *bin2-1-gof, dwf12-1D-gof* and *bin2-3 bil1 bil2* loss-of-function mutants was evaluated with respect to LR formation and expression of *LBD*s (Supplementary Fig. 2c,d). Compared with wild-type plants, in the presence of 1 μM auxin, *dwf12-1D-gof* mutants exhibited a 50% increase in LR density, whereas *bin2-3 bil1 bil2* triple mutants showed a 20% lower LR density (Fig. 3c). Compared with wild-type plants, *dwf12-1D-gof* consistently exhibited hypersensitivity to exogenous auxin in a time-dependent manner, as determined by the expression of *LBD16* and *LBD29*. However, *LBD16* and *LBD29* expression was reduced in the *bin2-3 bil1 bil2* mutant in the presence of exogenous auxin (Supplementary Fig. 2d). Consistently, bikinin treatment reduced *LBD* expression and auxin-mediated LR development in a dosage-dependent manner (Supplementary Fig. 2e and Fig. 3d). Taken together, these results suggested that BIN2 functions to increase auxin-responsive gene expression. Consistent with this mechanism, co-expression of wild-type BIN2 and the auxin-responsive reporter *pGH3–LUC* significantly induced reporter expression in a transient protoplast system[33] in a dose-dependent manner (Fig. 3e and Supplementary Fig. 2f). In addition, co-expression of a gain-of-function $BIN2^{E263K}$ (*dwf12-1D*) activated the *GH3* reporter more strongly than BIN2, and synergistically enhanced the reporter activity in the presence of auxin (Fig. 3e).

We then examined the ability of other *Arabidopsis* group II GSK3 proteins to regulate auxin signalling using the *pGH3–LUC* reporter system. Whereas BIN2-LIKE1 (BIL1) increased *GH3* promoter activity to the same degree as BIN2, BIL2 did not significantly enhance *GH3* expression (Supplementary Fig. 3a). Consistent with a positive regulatory function for BIL1, the *bil1* null mutant showed 10% fewer emerged LRs than wild-type plants (Supplementary Fig. 3b,c). As expected, both *bil1 bin2-3* and *bin2-3 bil1 bil2* loss-of-function mutants exhibited a similar reduction of approximately 20% in LR primordia density (Supplementary Fig. 3c). Taken together, these results indicate

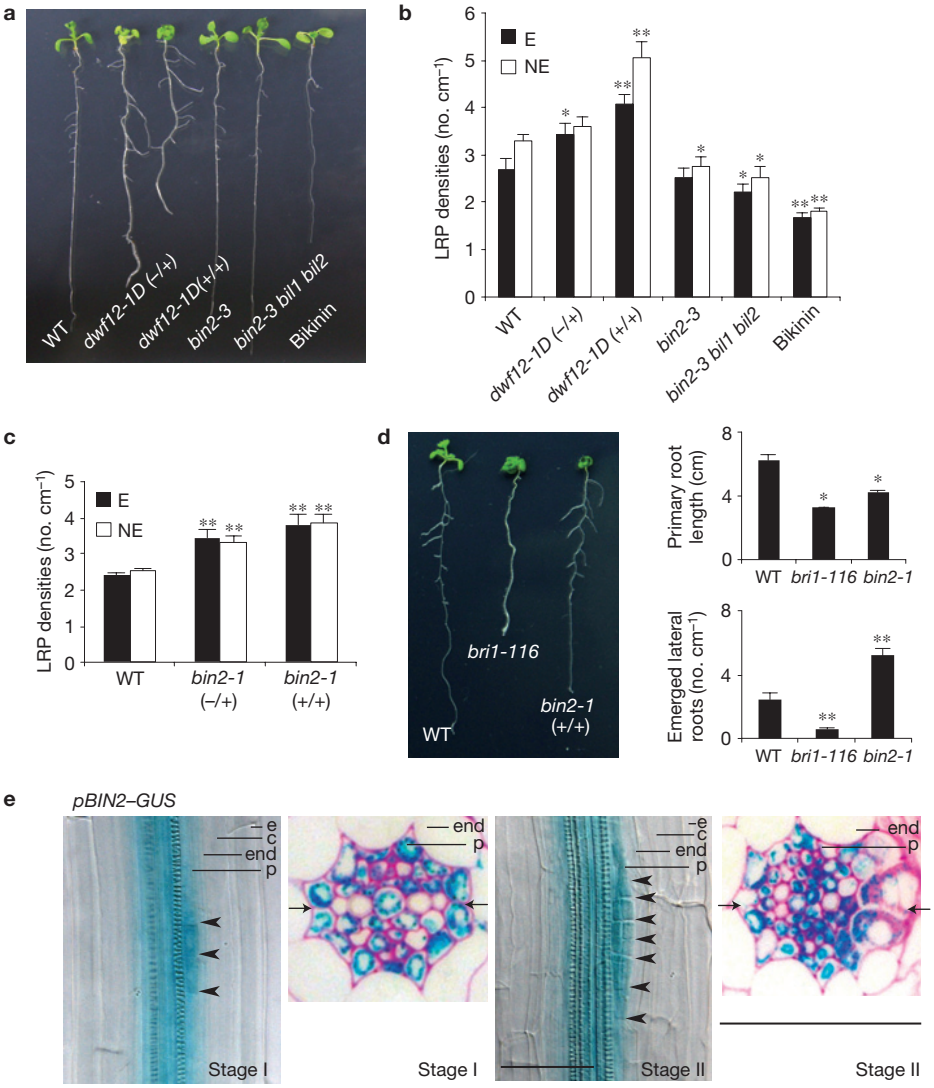

Figure 1 BIN2 positively regulates LR development. (**a**,**b**) BIN2 kinase activity is essential for proper LR development. Representative twelve-day-old wild-type (WT; Ws-2), *dwf12-1D-gof* (heterozygote (−/+) and homozygote (+/+)), and *bin2-3-lof*, *bin2-3 bil1 bil2* mutant and bikinin-treated seedlings are shown (**a**). LR primordium (LRP) densities. E, emerged LRs; NE, non-emerged LRP ($n = 15$ plants; **b**). (**c**) LRP densities of 12-day-old seedlings of wild-type (Col-0), *bin2-1-gof* heterozygote (−/+) and homozygote (+/+) mutant plants ($n = 12$ plants). (**d**) The LR development phenotype of 12-day-old seedlings of wild-type (Col-0), *bri1-116* and *bin2-1-gof* (left-panel). The primary root lengths and densities of emerged LRs in wild-type (Col-0), *bri1-116,* and *bin2-1-gof* (+/+; right panel; $n = 12$ plants). (**e**) *pBIN2–GUS* expression limited to LRP and vascular tissues at stage I and II (left panel, black arrowheads indicate dividing pericycle cells) and transverse sections of *pBIN2–GUS* seedlings through the LRP (right panel, black arrows indicate xylem pole pericycle cells). e, epidermis; c, cortex; end, endodermis; p, pericycle. Scale bars, 50 μm. Asterisks indicate statistically significant differences as compared with wild-type at $^{*}P < 0.05$ and $^{**}P < 0.01$. Error bars indicate s.e.m. For details on the statistical analysis, see the Methods.

that BIN2 and BIL1 function redundantly to stimulate auxin signalling during LR development.

To genetically dissect BIN2 action in auxin-mediated LR formation, *bin2-1-gof* was crossed with various auxin signalling defective mutants. For this purpose, the following alleles were used: *arf7-1* and *arf19-1* (loss-of-function alleles of *ARF7* and *ARF19*, respectively[10,31]), *tir1-1* (a loss-of-function allele of the auxin receptor *TIR1*; ref. 34), and *msg2-1* (a gain-of-function allele of *IAA19* encoding an auxin-insensitive, constitutively stable repressor protein[11]). The *bin2-1-gof* mutant slightly restored the *arf7-1* LR phenotype, which was possibly due to the presence of the functional ARF7 homologue, ARF19 (Fig. 3f and Supplementary Fig. 3d,e). Indeed, *bin2-1-gof* failed to rescue the *arf7-1 arf19-1* double-mutant lateral rootless phenotype (Fig. 3f). To exclude the possibility that alterations in TIR1-mediated degradation of AUX/IAAs caused the observed lack of suppression, *bin2-1*, *msg2-1 bin2-1-gof* and *tir1-1 bin2-1-gof* double mutants were analysed. *bin2-1-gof* rescued *msg2-1* and *tir1-1* LR phenotypes, as evidenced by the significant increase in emerged LR density (Fig. 3f,g). These results suggested that BIN2 functions either downstream of TIR1 or in parallel with TIR1-mediated auxin signalling during LR development. In addition, BIN2-mediated activation of LR development required ARF7 and ARF19. This prompted the hypothesis that BIN2 may relieve ARF7 and ARF19 from their repressor complex, thus leading to their activation irrespective of TIR1 activity during LR organogenesis.

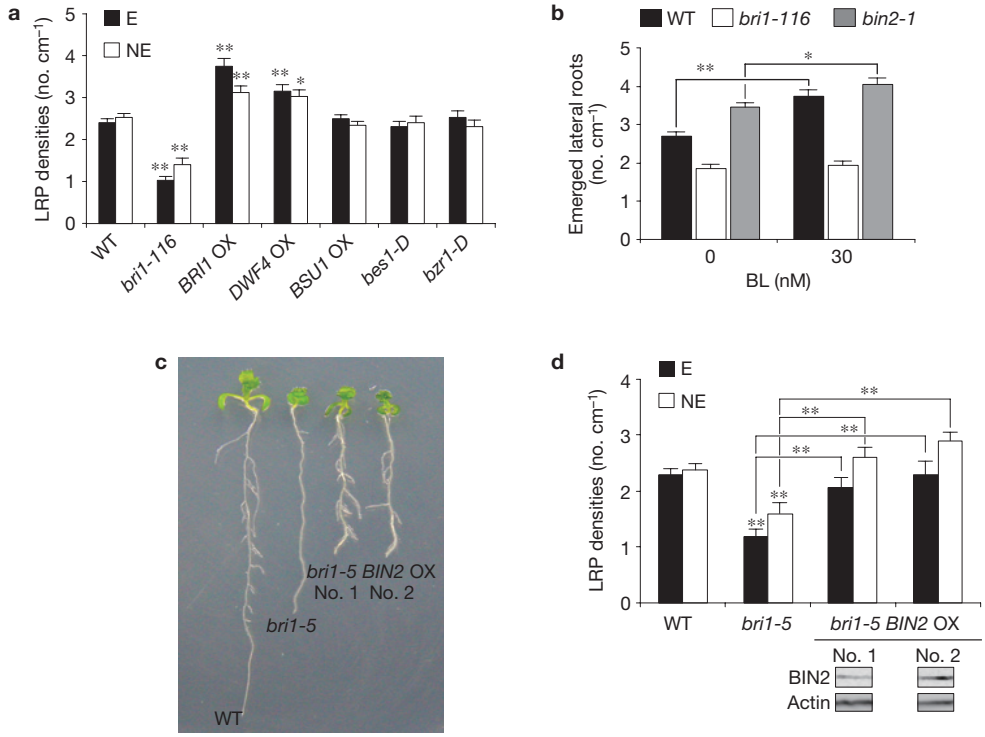

Figure 2 BR plays a minor role in BIN2-mediated LR development. (**a**) LRP densities of 12-day-old seedlings of wild-type (Col-0), *bri1-116*, *BRI1* overexpressing (OX), *DWF4* OX, *BSU1* OX, *bes1-D* (*pBES1–bes1-D–HA*) and *bzr1-D* mutants ($n = 15$ plants). (**b**) Different BL responses of *bri1-116* and *bin2-1-gof* (+/+) in LR development. Treatment: BL for 5 days ($n = 20$ plants). (**c**) The LR development phenotype of 12-day-old seedlings of wild-type (Ws-2), *bri1-5,* and *bri1-5 BIN2* OX. (**d**) LRP densities of 12-day-old seedlings of wild-type (Ws-2), *bri1-5,* and *bri1-5 BIN2* OX. BIN2–HA proteins in the transgenic plants are presented ($n = 12$ plants; lower). Error bars indicate s.e.m. ($^{*}P < 0.05$, $^{**}P < 0.01$ by Student's *t*-test). For details on the statistical analysis, see the Methods. A full scan image of the western blot is shown in Supplementary Fig. 8.

BIN2 directly phosphorylates ARF7 and ARF19

To elucidate the molecular mechanism of BIN2 action on auxin signal transduction, we examined whether BIN2 directly interacts with ARF or AUX/IAA proteins. In an *in vitro* pulldown assay with GST–BIN2, HA-tagged ARF7 was pulled down (Fig. 4a). Specifically, the QSL-rich carboxy-terminal domain, including the middle region and AUX/IAA dimerization domain (d2 ARF7), but not the B3 DNA-binding domain (d1 ARF7), directly interacted with BIN2 (Fig. 4b). In contrast, AUX/IAA proteins did not interact with BIN2 (Supplementary Fig. 4).

We next investigated whether ARF7 was phosphorylated by BIN2. BIN2, BIN2^{E263K} and BIL1 increased the intensity of high-molecular-weight bands of ARF7 in a gel shift assay (Fig. 4c). The higher-molecular-weight band shift of ARF7 was abolished by calf intestine alkaline phosphatase (CIAP) treatment (Fig. 4d), indicating that the ARF7 mobility shift was due to phosphorylation by BIN2. Conversely, a kinase-dead loss-of-function mutant BIN2^{K69R} and BIL2 failed to increase the intensity of the phosphorylated ARF7 band (Fig. 4c). In addition, phosphorylated ARF7 was highly enriched in *dwf12-1D-gof* plants (Fig. 4e), and BIN2 interacted with ARF19 and shifted the mobility of ARF19 proteins (Fig. 4f,g). *In vitro* kinase assays revealed that BIN2 induced the phosphorylation in the QSL-rich C-terminal domain of ARF7 (Fig. 4h). Liquid chromatography–tandem mass spectrometry (LC–MS/MS) analysis of the phosphorylated QSL-rich C-terminal domain of ARF7 showed that BIN2-dependent phosphorylation occurred at Ser 698 and Ser 707 (Fig. 4i). Taken together, these results suggest that BIN2 directly interacts with and phosphorylates ARF7 and ARF19.

BIN2-mediated phosphorylation induces ARF7 and ARF19 activity by attenuating their interaction with AUX/IAAs

Next, the ability of BIN2 to affect auxin signalling by modulating ARF7 and ARF19 activity through phosphorylation was investigated. BIN2 enhanced *pGH3–LUC* activity, and co-expression of *BIN2* with either *ARF7* or *ARF19* further enhanced reporter expression (Fig. 5a,b). In contrast, the kinase-dead BIN2^{K69R} mutant exerted a dominant-negative effect, reducing ARF7-induced activation of the reporter by 60% (Fig. 5a). These data indicate that BIN2 enhances ARF7- and ARF19-mediated transcriptional activation.

BIN2-mediated phosphorylation may enhance ARF7 activity by blocking its interaction with AUX/IAA repressors. Thus, we investigated whether phosphorylation by BIN2 affects the association of ARF7 with AUX/IAAs. Among the 29 members of *Arabidopsis* AUX/IAAs, IAA1, IAA3, IAA14, IAA18 and IAA19 are involved in LR initiation[32]. Whereas hypo-phosphorylated ARF7 proteins were precipitated together with GST–IAA1, GST–IAA3, GST–IAA14, GST–IAA18 and GST–IAA19, hyper-phosphorylated ARF7 proteins were only weakly pulled down with these AUX/IAA proteins in the presence of BIN2 (Fig. 5c and Supplementary Fig. 5). However, BIN2^{K69R} did not affect the association of ARF7 with AUX/IAA proteins (Fig. 5c). Furthermore, substitution of both Ser 698 and Ser 707 with alanine (ARF7$^{S698A/S707A}$, ARF7m) could not interfere with the

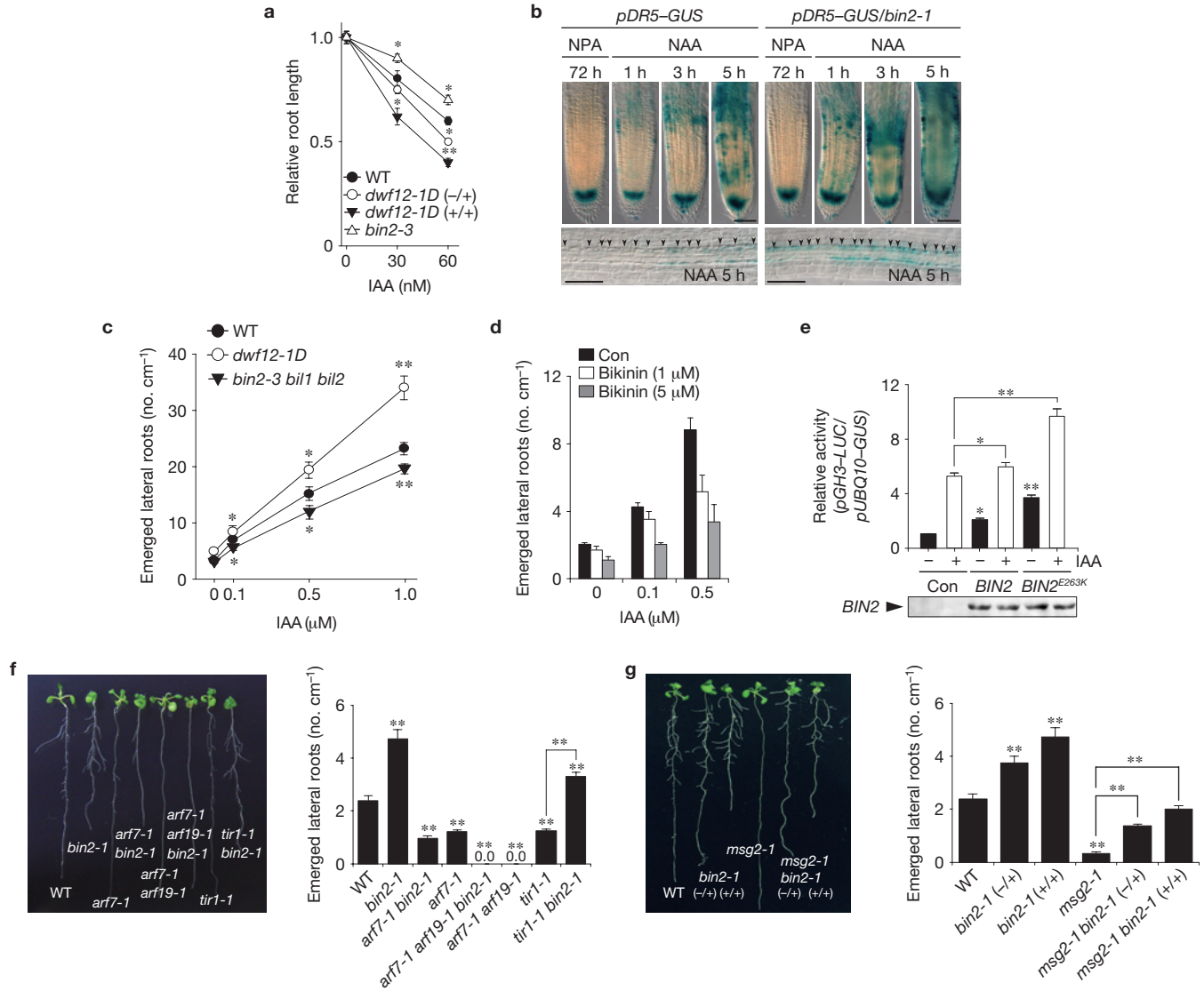

Figure 3 BIN2-mediated signalling is integrated into ARF7/19 during LR development. (**a**) Different auxin responses of *bin2* mutants in root elongation. Relative root length of the 12-day-old *dwf12-1D-gof* (heterozygote (−/+) and homozygote (+/+)) and *bin2-3-lof* compared with wild-type. Treatment: IAA for 5 days ($n = 12$ plants). (**b**) The *bin2-1-gof* mutation increases auxin sensitivity in *pDR5–GUS* activation. The indicated plants were grown for 72 h in the presence of 10 μM NPA and then transferred to 1 μM NAA for 1, 3 and 5 h. The arrowheads indicate dividing pericycle cells. Scale bars, 50 μm. (**c**) BIN2 increases auxin sensitivity in LR formation. The densities of emerged LRs in 11-day-old seedlings of wild-type (Ws-2), *dwf12-1D-gof* homozygote (+/+), and *bin2-3 bil1 bil2* mutant. Treatment: IAA for 4 days ($n = 12$ plants). (**d**) Bikinin treatment inhibits auxin-mediated LR development. The densities of emerged LRs were measured in the presence of the indicated concentrations of auxin and bikinin. ($n = 15$ plants). (**e**) BIN2 and auxin synergistically enhance the activity of the GH3 promoter. Protoplasts were co-transfected with pUBQ10–GUS (internal control), *pGH3–LUC* and the indicated effector constructs, and treated with 1 μM IAA for 3 h. BIN2 protein levels were detected using anti-HA antibody ($n = 4$, 20,000 cells per $n = 1$). A full scan image of the western blot is shown in Supplementary Fig. 8. For statistics source data, see Supplementary Table 2. (**f**) *bin2-1-gof* homozygote mutation suppresses the LR defects of *tir1-1*, but not *arf7-1*, and *arf7-1 arf19-1*. The densities of the emerged LRs of 12-day-old seedlings of indicated genotypes are presented ($n = 16$ plants). (**g**) *bin2-1-gof* partially suppresses the defective LR phenotype of *msg2-1*. The densities of the emerged LRs of 12-day-old seedlings of indicated genotypes are presented ($n = 15$ plants). Error bars indicate s.e.m. ($^*P < 0.05$, $^{**}P < 0.01$ by Student's *t*-test). For details of the statistical analysis, see the Methods.

interaction with AUX/IAA proteins in the absence and presence of BIN2 (Fig. 5c). We then examined whether phosphorylation affects ARF7-mediated auxin response. ARF7m itself was able to activate *pGH3–LUC* as much as wild-type ARF7, and its repressor IAA19 inhibited the activity of the reporter (Fig. 5d). Interestingly, IAA19 suppression of the reporter activity was compromised by BIN2 together with ARF7, but not with ARF7m. Consistently, overexpression of *ARF7* in *arf7-1* (referred to as *ARF7 arf7-1*) restored the LR defects of *arf7-1* to wild–type levels, but *ARF7m* overexpression in three independent *ARF7* transgenic plants with similar protein levels (referred to as *ARF7m arf7-1*) only partially recovered the LR defects of *arf7-1* (Fig. 5e). Furthermore, *bin2-1-gof* increased the LR formation of *ARF7 arf7-1* transgenic plants, but not *ARF7m arf7-1* plants (Fig. 5f). We therefore concluded that BIN2-mediated phosphorylation of ARF7 attenuates the interaction of ARF7 with AUX/IAAs and leads to the activation of auxin signalling. The ability of BIN2-mediated phosphorylation to

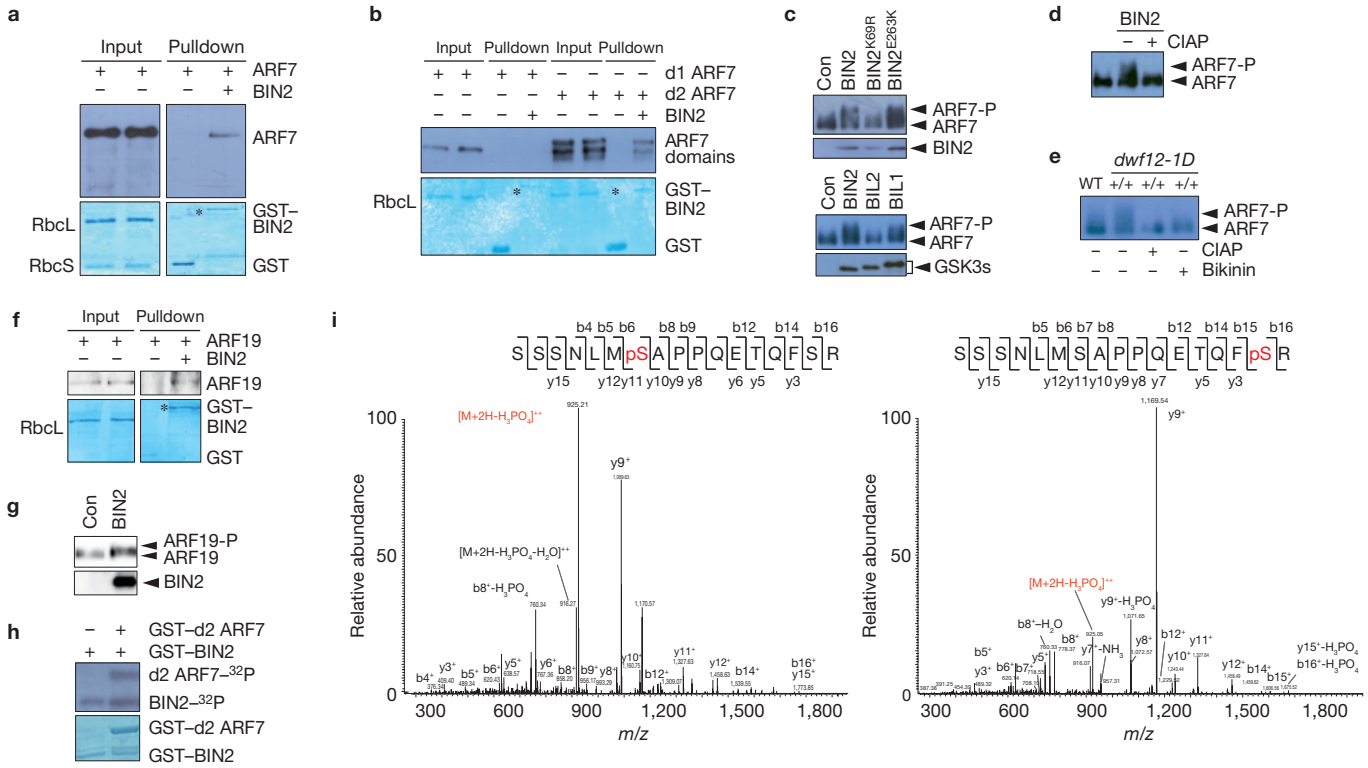

Figure 4 BIN2 directly phosphorylates ARF7. (**a**) BIN2 interacts with ARF7. Protoplast lysates overexpressing *ARF7–HA* were incubated with purified GST–BIN2 proteins and pulled down with glutathione Sepharose 4B. GST–BIN2-bound proteins were visualized with anti-HA HRP antibody. An asterisk indicates GST–BIN2 proteins. (**b**) BIN2 interacts with the QSL-rich C-terminal domain of ARF7 (d2 ARF7). Protoplast lysates overexpressing the HA-tagged B3 DNA-binding domain of *ARF7* (*d1 ARF7*) or QSL-rich C-terminal domain (*d2 ARF7*) were incubated with GST–BIN2 or GST proteins and pulled down with glutathione Sepharose 4B. Precipitated proteins were visualized by anti-HA antibody. (**c**) BIN2 kinase activity is required for ARF7 phosphorylation. HA-tagged ARF7 was co-transfected into protoplasts with *BIN2–HA*, *BIN2*^{E263K}*–HA*, *BIN2*^{K69R}*–HA* or *BIL1–HA*, *BIL2–HA*. After 6 h of transfection, the indicated proteins were visualized with anti-HA antibody. (**d**) The BIN2-induced mobility shift was abolished by CIAP treatment. (**e**) ARF7 is phosphorylated by BIN2 *in vivo*. The phosphorylation status of ARF7 proteins in wild-type, *dwf12-1D-gof* plants harbouring *35S–ARF7–HA* in the presence or absence of 5 μM bikinin. The BIN2-induced mobility shift was abolished by CIAP or bikinin treatment. (**f**) BIN2 interacts with ARF19 *in vitro*. Protoplast lysates overexpressing *ARF19–HA* were incubated with GST–BIN2 proteins and pulled down with glutathione Sepharose 4B. GST–BIN2-bound proteins were visualized with anti-HA HRP antibody. An asterisk indicates GST–BIN2 proteins. (**g**) BIN2 phosphorylates ARF19 proteins. *ARF19–HA* was co-transfected into protoplasts with *BIN2–HA*. ARF19 and BIN2 proteins were visualized with anti-HA antibody. (**h**) BIN2 directly phosphorylates ARF7. GST-tagged BIN2 and the QSL-rich C-terminal domain of ARF7 (d2 ARF7) were used in an *in vitro* kinase assay. The autoradiogram shows protein phosphorylation (upper panel). The protein levels were determined by Coomassie blue staining (lower panel). (**i**) MS/MS spectra for two major phosphopeptides of GST–d2 ARF7 showing *in vitro* BIN2 phosphorylation sites of ARF7 at Ser 698 (left panel) and Ser 707 (right panel). GST–d2 ARF7 was incubated with GST–BIN2 and ATP for 12 h. The proteins were digested by trypsin and analysed by LC–MS/MS. Full scan images of western blots are shown in Supplementary Fig. 8.

alter the interaction between ARF7 and IAA19 was further supported by the rescue of *msg2-1* by *bin2-1-gof* (Fig. 3g).

We next investigated whether AUX/IAAs dissociated from phosphorylated ARFs could be more rapidly degraded through the TIR1 pathway. To test this possibility, the effect of ARF7 phosphorylation on the relative amount of interacting proteins in TIR1–ARF7–IAA19 complexes was tested. Co-expression of *BIN2* attenuated the interaction of IAA19 with ARF7, and BIN2 increased the interaction of IAA19 with TIR1 (Fig. 6a and Supplementary Fig. 6a). We then examined the protein level of IAA19 in wild-type or *bin2-1-gof* plants. The proteolysis of IAA19 proteins occurred more rapidly in *bin2-1-gof* than in wild-type plants, but bikinin treatment effectively inhibited the IAA19 protein degradation (Fig. 6b). Consistently, the fluorescence of DII–VENUS, which has no dimerization domain with ARFs, was not significantly affected by bikinin treatment (Supplementary Fig. 6b). These results suggested that BIN2-mediated phosphorylation of ARF7 diminishes its interaction with AUX/IAA proteins and subsequently enlarges the pool of free ARF7 proteins by facilitating degradation of their repressor AUX/IAAs.

We next examined whether BIN2-mediated phosphorylation of ARF7 and ARF19 affects their binding to target promoters using a chromatin immunoprecipitation assay. Whereas DNA binding of ARF7 and ARF19 to the promoters of *LBD16* and *LBD29* was increased in the presence of auxin, bikinin treatment suppressed the auxin-induced enhancement of DNA binding (Fig. 6c,e). Furthermore, the *dwf12-1D-gof* enhanced DNA binding of ARF7 to their target promoters (Fig. 6d). The *bin2-1-gof* further increased auxin-induced enhancement of ARF19 binding, but bikinin treatment compromised the enhancement of ARF19 binding in *bin2-1-gof*, to the *LBD29* promoter (Fig. 6f). Together, these results indicated that phosphorylation of ARFs could increase the pool of active ARFs by attenuating the interaction with AUX/IAAs and enhance their DNA-binding capacity.

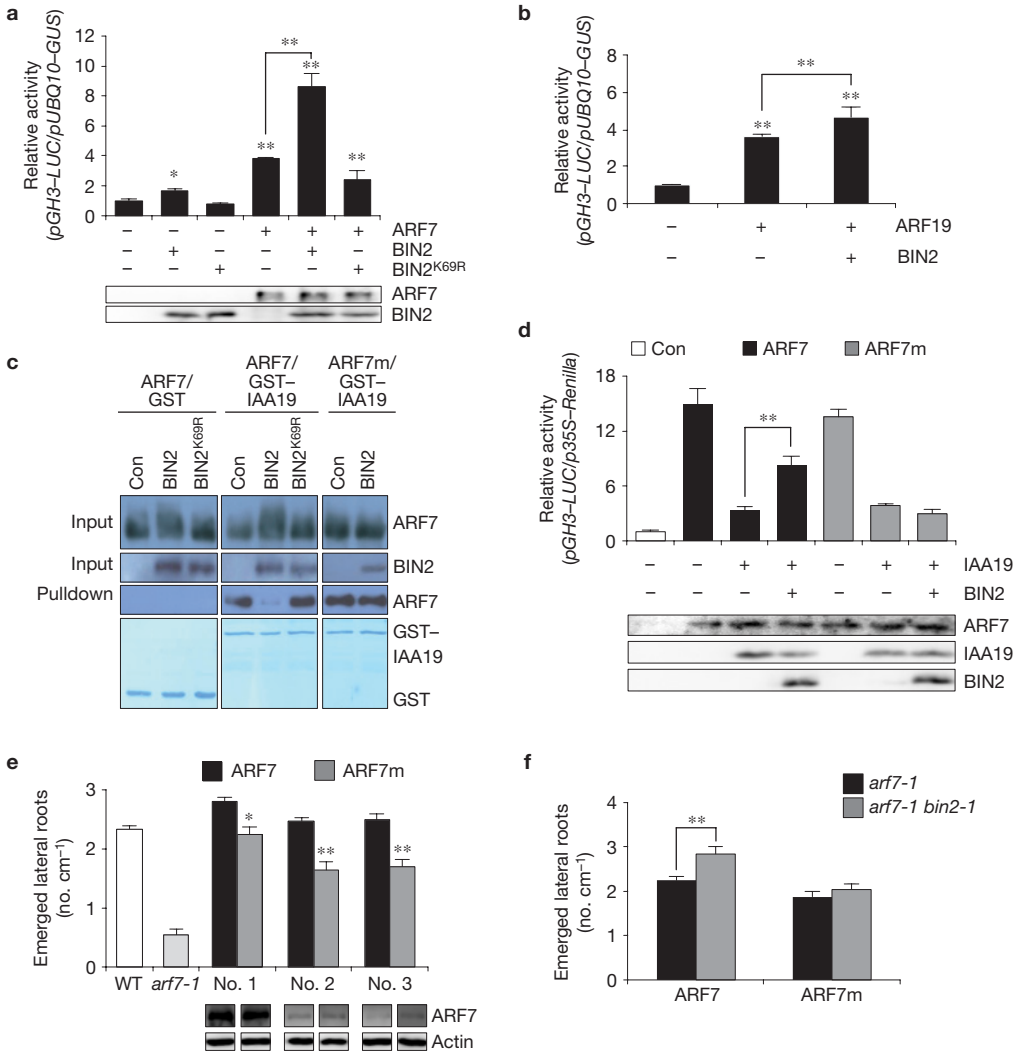

Figure 5 BIN2 attenuates the interaction of ARF7 with AUX/IAAs and enhances its transcriptional activity, leading to activation of auxin response. (**a**) BIN2 enhances the transcriptional activity of ARF7. The relative fold induction of luciferase activity was determined ($n = 4$, 20,000 cells per $n = 1$). Protein expression levels are presented (lower). (**b**) BIN2 enhances the transcriptional activity of ARF19. The relative fold induction of luciferase activity was determined ($n = 4$, 20,000 cells per $n = 1$). (**c**) BIN2-mediated phosphorylation of ARF7 represses its interaction with IAA19, but mutation of two phosphorylation sites of ARF7 (ARF7m: ARF7$^{S698A/S707A}$) blocks BIN2-mediated dissociation with IAA19. (**d**) BIN2 could not enhance the transcriptional activity of ARF7m in the presence of IAA19 in protoplasts ($n = 4$, 20,000 cells per $n = 1$). ARF7, IAA19 and BIN2 protein levels were detected using anti-HA antibody. (**e**) The LR defects of *arf7-1* are completely rescued by overexpression of *ARF7*, but partially by *ARF7m* ($n = 25$ plants). ARF7–HA and ARF7m–HA proteins in the transgenic plants are presented (lower). (**f**) The *bin2-1-gof* mutation enhanced ARF7-mediated LR formation, but not ARF7m. The densities of LRs of wild-type, *arf7-1 35S–ARF7–HA (bin2-1-gof)* and *arf7-1 35S–ARF7m–HA* (*bin2-1-gof*) are presented ($n = 42$ plants). Error bars indicate s.e.m. ($^*P < 0.05$, $^{**}P < 0.01$ by Student's *t*-test). Full scan images of western blots are shown in Supplementary Fig. 8. For details on the statistical analysis, see the Methods.

TDIF–TDR signalling module affects BIN2 during LR development

Our results suggested that BIN2 action is directly linked to ARF transcription factors, but the limited role of BR-mediated regulation of BIN2 in LR development suggested that other regulatory components could impact on BIN2 activity during this process. To identify other upstream regulators of BIN2-mediated LR development, we screened for BIN2-interacting proteins using a yeast two-hybrid system and identified TDR as a potential interacting partner. TDR is known to function as a receptor of TDIF (CLE41 and CLE44) peptide in vascular bundle development[35]. Yeast two-hybrid assays showed that BIN2 interacts with the kinase domain of TDR (TDR kd; Fig. 7a). Furthermore, we could pulldown full-length TDR proteins with GST-tagged BIN2 (Fig. 7b). This interaction suggested that TDR might be involved in LR development through the regulation of BIN2. To investigate this possibility, we first examined the expression pattern of *pTDR–GUS* in roots. *TDR* was expressed in the vasculature, in pericycle cells and during LR initiation, which overlapped with *BIN2* expression (Figs 1e and 7c). Consistently, a loss-of-function *tdr* mutant exhibited altered LR density compared with wild-type plants (Fig. 7d).

We then investigated whether the TDIF–TDR signalling module plays a role in BIN2-mediated LR development. The LR density of wild-type plants increased following TDIF treatment in a dosage-dependent manner (Fig. 7d). However, inhibition of BIN2 activity by bikinin

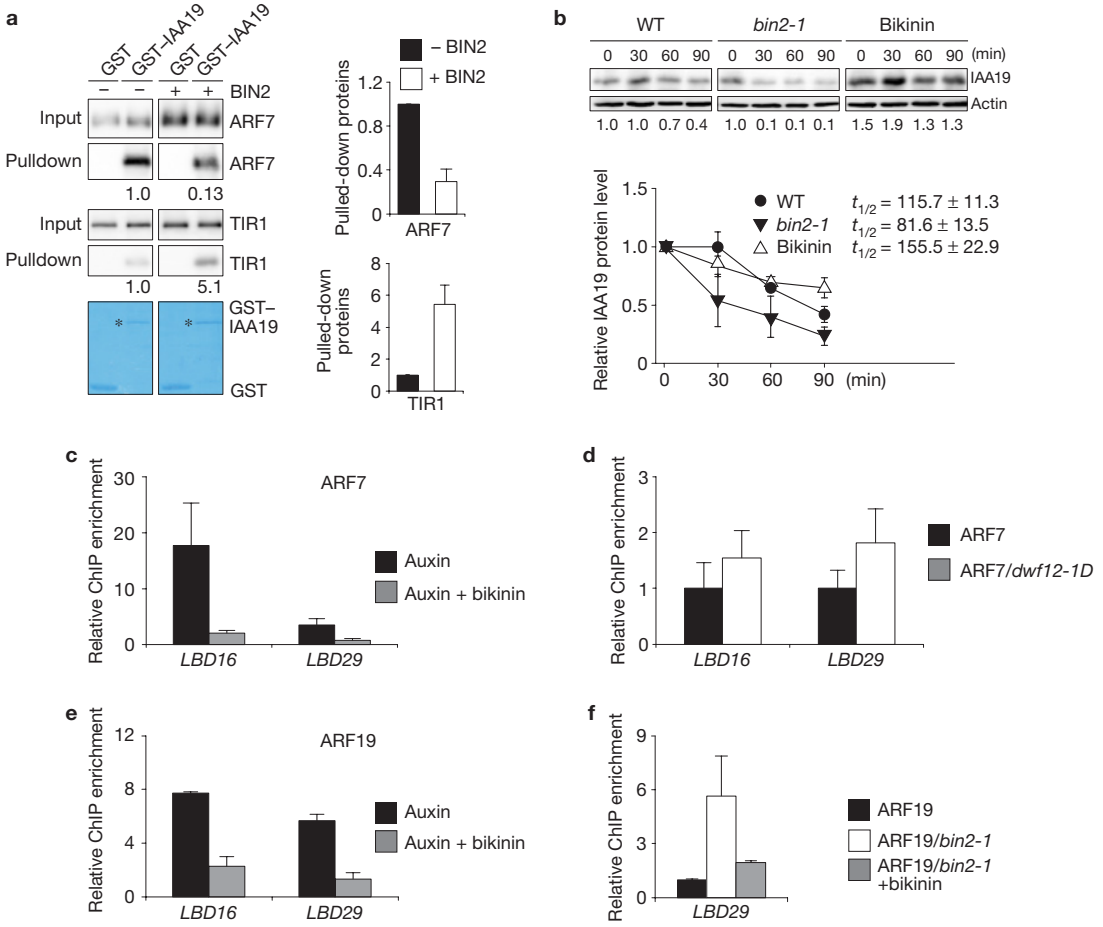

Figure 6 BIN2 increases DNA-binding capacity of ARF7 and ARF19. (**a**) BIN2-mediated phosphorylation of ARF7 results in increased binding of IAA19 with TIR1. Asterisks indicate GST–IAA19 proteins. The levels of GST–IAA19 pulled-down proteins were normalized to those of the input proteins. The normalized intensities of the pulled-down proteins in the absence of BIN2 were set to 1, and the relative protein intensities are presented under the corresponding protein bands (left panel). The average values of the relative band intensities from three independent experiments are plotted (right panel). (**b**) IAA19 proteins are rapidly degraded in *bin2-1-gof* plants but stabilized by bikinin. Wild-type (Col-0) and *bin2-1-gof* homozygote plants expressing *35S–IAA19–HA* were grown in the presence of 5 μM bikinin or mock control, and incubated for the indicated times with 100 μM cycloheximide. The levels of IAA19 proteins were determined with anti-HA antibody (upper panel). The average value of IAA19 band intensities and half-life of IAA19 proteins from three independent experiments was calculated (lower panel). ($n = 3$, 10 plants per $n = 1$). For statistics source data, see Supplementary Table 2. (**c**–**f**) BIN2 increases the binding of ARFs to the *LBD16* and *LBD29* promoters. A BIN2 inhibitor, bikinin, represses the binding of ARF7 and ARF19 to the *LBD16* and *LBD29* promoters (**c**,**e**). The *dwf12-1D-gof* and *bin2-1-gof* mutations enhance the DNA binding of ARF7 and ARF19 to the *LBD16* and *LBD29* promoter (**d**,**f**). The DNA binding of ARF7 and ARF19 was determined by quantitative RT–PCR. Error bars indicate s.e.m. ($n = 6$ for ARF7, $n = 4$ for ARF19, 200 plants per $n = 1$). The *LBD29* promoters bound to ARF19 proteins in *bin2-1-gof* were determined with/without 50 μM bikinin in the presence of 1 μM 2.4D. For source data, see Supplementary Table 2. Full scan images of western blots are shown in Supplementary Fig. 8.

treatment or a loss-of-function *tdr* mutation completely suppressed the positive effect of TDIF on LR development (Fig. 7d). TDIF treatment increased the phosphorylation of ARF7 in plants, and its functional receptor, TDR, was required for the phosphorylation. However, bikinin completely blocked TDIF-mediated phosphorylation of ARF7 (Fig. 7e). Furthermore, TDIF increased the LR density of only *arf7-1* mutants expressing wild-type *ARF7*, but not *mARF7* (Fig. 7f). Exogenous TDIF further increased LR formation in *bin2-1-gof* compared with wild-type plants, but *bin2-3-lof* rarely responded to TDIF (Fig. 7g). These results implied that TDIF–TDR signalling could affect the transcriptional activity of ARF7 by BIN2-mediated phosphorylation. To examine this idea, we determined the effects of the TDIF–TDR signalling module on ARF7-mediated activation of *pGH3–LUC*. Interestingly, exogenous TDIF or expression of *TDR* itself did not affect the *pGH3–LUC* activity, but TDIF treatment significantly promoted the reporter activity in the presence of TDR (Fig. 7h). Furthermore, ARF7-mediated reporter activation was enhanced by BIN2, and co-expression of *TDR* with TDIF treatment further increased BIN2-mediated activation of ARF7 activity. These data indicated that the TDIF–TDR module affects BIN2-mediated auxin signalling output during LR organogenesis.

DISCUSSION

Auxin is involved in nearly every aspect of plant development through a relatively simple signalling circuit in which de-repression of ARFs following auxin perception activates a transcriptional response[1]. However, it has been uncertain how auxin could provide a wide range of signalling outputs for plant growth and development. For example, several combinations of auxin co-receptor machineries, especially

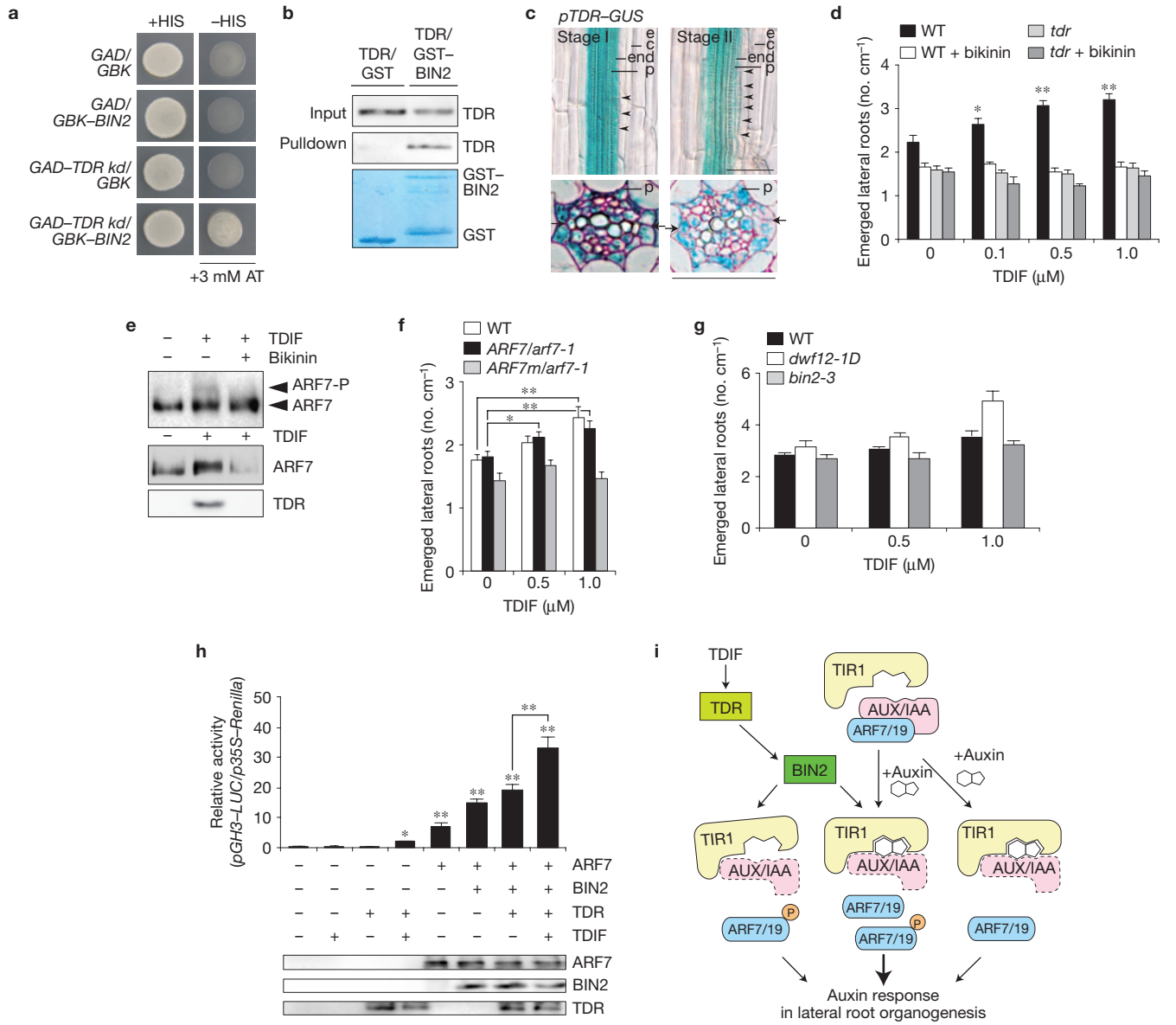

Figure 7 TDIF–TDR module is directly linked to BIN2-mediated auxin signal activation in LR development. (**a**) BIN2 interacts with the TDR kd in a yeast two-hybrid assay. (**b**) BIN2 interacts with TDR. Protoplast lysates overexpressing *TDR–HA* were incubated with purified GST–BIN2 proteins and pulled down with glutathione Sepharose 4B. An asterisk indicates GST–BIN2 proteins. (**c**) *pTDR–GUS* expression limited to LRP and vascular tissues at stage I and II (upper panel, black arrowheads indicate dividing pericycle cells) and transverse sections of *pTDR–GUS* seedlings through the LRP (lower panel, black arrows indicate xylem pole pericycle cells). e, epidermis; c, cortex; end, endodermis; p, pericycle. Scale bars, 50 μm. (**d**) TDR is positively involved in LR development in a GSK3-dependent manner. The densities of emerged LRs of seedlings treated with the indicated concentrations of TDIF with/without 5 μM bikinin ($n = 15$ plants). (**e**) TDIF induces the phosphorylation of ARF7. *35S–ARF7–HA* transgenic plants were treated with 1 μM TDIF in the absence or presence of 5 μM bikinin (upper panel). HA-tagged *ARF7* was co-transfected into protoplasts with or without *TDR–MYC*. After 5 h of transfection, the protoplasts were further incubated with 1 μM TDIF for 1 h (lower panel). (**f**) TDIF increases LR development by BIN2-mediated phosphorylation of ARF7. The densities of the emerged LRs of indicated genotypes are presented ($n = 15$ plants). (**g**) The densities of emerged LRs of wild-type (Ws-2), *dwf12-1D-gof* (+/+) and *bin2-3-lof* treated with the indicated concentrations of TDIF ($n = 15$ plants). (**h**) TDIF–TDR–BIN2 cascade enhances the transcriptional activity of ARF7 in protoplasts ($n = 4$, 20,000 cells per $n = 1$). ARF7, BIN2 and TDR protein levels were detected using anti-HA or anti-MYC antibody. Error bars indicate s.e.m. ($^{*}P < 0.05$, $^{**}P < 0.01$ by Student's t-test). (**i**) A model for the TDIF–TDR–BIN2-mediated regulatory module of auxin signal transduction. Full scan images of western blots are shown in Supplementary Fig. 8. For details on the statistical analysis, see the Methods.

between TIR1/AFB receptors and AUX/IAA repressors, could modulate auxin sensitivity[6]. Our study revealed another regulatory module in auxin signalling that involves phosphorylation-dependent regulation of transcriptional activity of ARFs during LR development through the TDIF–TDR–BIN2 signalling cascade.

BIN2 associated with the TDIF–TDR module positively regulates auxin-mediated LR development by phosphorylating ARF7 and ARF19. This alleviates the interaction between these ARFs and AUX/IAAs, facilitates SCF^{TIR1}-mediated degradation of AUX/IAAs, and eventually enhances transcriptional activity of ARFs, possibly by preventing

the reformation of an ARF–AUX/IAA complex and consequently increasing the pool of free ARF proteins. BIN2 phosphorylates ARF2 *in vitro*[23] and ARF7 *in vivo* (Fig. 4e), but the two identified phosphorylation residues in ARF7 are not conserved in ARF2 and other ARF transcriptional activators, although ARF proteins do harbour many putative GSK3 phosphorylation sites. Interestingly, BIN2-mediated phosphorylation of ARF7 and ARF19 enhances their DNA-binding capacity (Fig. 6), whereas—in contrast—ARF2 phosphorylation reduces its DNA-binding and repressor activity[23]. The regulation of ARF DNA binding by its phosphorylation is likely to be a critical regulatory mechanism for diversity and specificity of auxin signalling during plant growth and development.

BR and auxin interact synergistically during various physiological responses[36]. However, this study revealed that BIN2, a negative regulator in BR signalling, positively regulates auxin signalling during LR development. BRI1, a major BR receptor, is involved in BR-mediated activation of LR development, but the canonical BR signalling output determined by BSU1, a BIN2 repressor, and downstream components BES1 and BZR1 are probably not involved in LR development (Fig. 2). It is plausible that a not-yet identified signalling pathway bifurcated from BRI1-mediated BR signalling enhances auxin transport, leading to stimulation of LR development[37]. Furthermore, BR did not affect BIN2-induced phosphorylation or transcriptional activity of ARF7, but a GSK3 inhibitor suppressed BIN2-mediated activation of auxin signalling (Supplementary Fig. 7). These data demonstrate that BR probably plays a minor role, if any, in the regulation of BIN2 activity during LR development. Importantly, the group II GSK3 proteins seem to have a functional redundancy in BR signalling pathways[26], but only BIN2 and BIL1 showed positive roles in ARF7- and ARF19-mediated LR development (Supplementary Fig. 3), which suggests specificity of GSK3 proteins in diverse developmental processes.

In *Arabidopsis*, cell–cell regulation through small secreted peptides and their receptors is essential for various developmental processes[38]. For example, TDIF–TDR controls xylem differentiation and proliferation of procambium for vascular bundle development[35], and TDIF and its related peptide, CLE42, are also involved in axillary meristem formation and bud outgrowth[39]. Here, we showed that the TDIF–TDR signalling module also regulates LR development through BIN2-mediated control of auxin signalling. Interestingly, *TDIF* is mainly expressed in the phloem and its expression is activated by auxin[40]. This expression pattern suggests that auxin-induced TDIF peptides in the phloem move to the pericycle and stimulate the TDR–BIN2 module, reinforcing auxin signalling for positioning and development of LRs.

Taken together, these events triggered by TDIF–TDR–BIN2 signalling cues could increase the pool of active ARF7 and ARF19, in harmony with auxin-induced degradation of IAA proteins, strengthening the signalling output of auxin during LR organogenesis (Fig. 7i). This peptide-initiated phosphorylation-mediated control of transcriptional activity of ARFs provides a broad spectrum of auxin signalling outputs to specific cells with a graded distribution of auxin during various development processes. Our results also suggest that a TDIF–TDR–GSK3-mediated regulatory module of ARFs is an important node for connecting diverse signalling networks in auxin-driven plant growth and development. □

METHODS

Methods and any associated references are available in the online version of the paper.

Note: Supplementary Information is available in the online version of the paper

ACKNOWLEDGEMENTS

The authors thank D. Weijers for critical reading of the manuscript and useful suggestions. This work was supported by grants from the Advanced Biomass R&D Center (2010-0029720) and the National Research Foundation (20110000212) funded by the Korean Ministry of Education, Science and Technology. H.R. was supported by grants from the Next-Generation BioGreen 21 Program (PJ009516). H.C. and S.H. were recipients of a Brain Korea 21 fellowship. I.D.S. was supported by a BBSRC David Phillips Fellowship (BB_BB/H022457/1) and a Marie Curie European Reintegration Grant (PERG06-GA-2009-256354).

AUTHOR CONTRIBUTIONS

H.C., H.R., S.H., J.P., K.H. and S.S. performed experiments. H.C., H.R., I.D.S. and I.H. designed experiments and analysed the data. D.A. analysed gene expression. S.R. and D.H. performed LC–MS/MS analysis. H.C., H.R., T.B., M.J.B., I.D.S. and I.H. wrote the manuscript.

COMPETING FINANCIAL INTERESTS

The authors declare no competing financial interests.

Published online at www.nature.com/doifinder/10.1038/ncb2893
Reprints and permissions information is available online at www.nature.com/reprints

1. Vanneste, S. & Friml, J. Auxin: a trigger for change in plant development. *Cell* **136,** 1005–1016 (2009).
2. Dharmasiri, N., Dharmasiri, S. & Estelle, M. The F-box protein TIR1 is an auxin receptor. *Nature* **435,** 441–445 (2005).
3. Kepinski, S. & Leyser, O. The *Arabidopsis* F-box protein TIR1 is an auxin receptor. *Nature* **435,** 446–451 (2005).
4. Lau, S., Jurgens, G. & De Smet, I. The evolving complexity of the auxin pathway. *Plant Cell* **20,** 1738–1746 (2008).
5. Szemenyei, H., Hannon, M. & Long, J. A. TOPLESS mediates auxin-dependent transcriptional repression during *Arabidopsis* embryogenesis. *Science* **319,** 1384–1386 (2008).
6. Villalobos, L. I. A. C. *et al.* A combinatorial TIR1/AFB-Aux/IAA co-receptor system for differential sensing of auxin. *Nat. Chem. Biol.* **8,** 477–485 (2012).
7. De Rybel, B. *et al.* A novel aux/IAA28 signaling cascade activates GATA23-dependent specification of lateral root founder cell identity. *Curr. Biol.* **20,** 1697–1706 (2010).
8. De Smet, I. Lateral root initiation: one step at a time. *New Phytol.* **193,** 867–873 (2012).
9. De Smet, I. *et al.* Bimodular auxin response controls organogenesis in *Arabidopsis*. *Proc. Natl Acad. Sci. USA* **107,** 2705–2710 (2010).
10. Okushima, Y., Fukaki, H., Onoda, M., Theologis, A. & Tasaka, M. ARF7 and ARF19 regulate lateral root formation via direct activation of LBD/ASL genes in *Arabidopsis*. *Plant Cell* **19,** 118–130 (2007).
11. Tatematsu, K. *et al.* MASSUGU2 encodes Aux/IAA19, an auxin-regulated protein that functions together with the transcriptional activator NPH4/ARF7 to regulate differential growth responses of hypocotyl and formation of lateral roots in *Arabidopsis thaliana*. *Plant Cell* **16,** 379–393 (2004).
12. Clevers, H. Wnt/β-catenin signaling in development and disease. *Cell* **127,** 469–480 (2006).
13. Dornelas, M. C., Wittich, P., von Recklinghausen, I., van Lammeren, A. & Kreis, M. Characterization of three novel members of the *Arabidopsis* SHAGGY-related protein kinase (ASK) multigene family. *Plant Mol. Biol.* **39,** 137–147 (1999).
14. Saidi, Y., Hearn, T. J. & Coates, J. C. Function and evolution of 'green' GSK3/Shaggy-like kinases. *Trends Plant Sci.* **17,** 39–46 (2012).
15. Kim, T. W., Michniewicz, M., Bergmann, D. C. & Wang, Z. Y. Brassinosteroid regulates stomatal development by GSK3-mediated inhibition of a MAPK pathway. *Nature* **482,** 419–422 (2012).
16. Li, J. M. & Nam, K. H. Regulation of brassinosteroid signaling by a GSK3/SHAGGY-like kinase. *Science* **295,** 1299–1301 (2002).
17. Gudesblat, G. E. *et al.* SPEECHLESS integrates brassinosteroid and stomata signalling pathways. *Nat. Cell Biol.* **14,** 548–554 (2012).
18. Ryu, H. *et al.* Nucleocytoplasmic shuttling of BZR1 mediated by phosphorylation is essential in *Arabidopsis* brassinosteroid signaling. *Plant Cell* **19,** 2749–2762 (2007).
19. Wang, Z. Y. *et al.* Nuclear-localized BZR1 mediates brassinosteroid-induced growth and feedback suppression of brassinosteroid biosynthesis. *Dev. Cell* **2,** 505–513 (2002).
20. Yin, Y. *et al.* BES1 accumulates in the nucleus in response to brassinosteroids to regulate gene expression and promote stem elongation. *Cell* **109,** 181–191 (2002).

21. Kim, T. W. *et al*. Brassinosteroid signal transduction from cell-surface receptor kinases to nuclear transcription factors. *Nat. Cell Biol.* **11,** 1254–1260 (2009).
22. Perez-Perez, J. M., Ponce, M. R. & Micol, J. L. The UCU1 *Arabidopsis* gene encodes a SHAGGY/GSK3-like kinase required for cell expansion along the proximodistal axis. *Dev. Biol.* **242,** 161–173 (2002).
23. Vert, G., Walcher, C. L., Chory, J. & Nemhauser, J. L. Integration of auxin and brassinosteroid pathways by Auxin Response Factor 2. *Proc. Natl Acad. Sci. USA* **105,** 9829–9834 (2008).
24. Choe, S. *et al*. Arabidopsis brassinosteroid-insensitive *dwarf12* mutants are semidominant and defective in a glycogen synthase kinase 3β-like kinase. *Plant Physiol.* **130,** 1506–1515 (2002).
25. Li, J., Nam, K. H., Vafeados, D. & Chory, J. BIN2, a new brassinosteroid-insensitive locus in *Arabidopsis*. *Plant Physiol.* **127,** 14–22 (2001).
26. Yan, Z., Zhao, J., Peng, P., Chihara, R. K. & Li, J. BIN2 functions redundantly with other *Arabidopsis* GSK3-like kinases to regulate brassinosteroid signaling. *Plant Physiol.* **150,** 710–721 (2009).
27. De Rybel, B. *et al*. Chemical inhibition of a subset of *Arabidopsis thaliana* GSK3-like kinases activates brassinosteroid signaling. *Chem. Biol.* **16,** 594–604 (2009).
28. Choi, S. *et al*. BAT1, a putative acyltransferase, modulates brassinosteroid levels in *Arabidopsis*. *Plant J.* **73,** 380–391 (2012).
29. Nam, K. H. & Li, J. BRI1/BAK1, a receptor kinase pair mediating brassinosteroid signaling. *Cell* **110,** 203–212 (2002).
30. Ryu, H., Kim, K., Cho, H. & Hwang, I. Predominant actions of cytosolic BSU1 and nuclear BIN2 regulate subcellular localization of BES1 in brassinosteroid signaling. *Mol. Cells* **29,** 291–296 (2010).
31. Okushima, Y. *et al*. Functional genomic analysis of the AUXIN RESPONSE FACTOR gene family members in *Arabidopsis thaliana*: unique and overlapping functions of ARF7 and ARF19. *Plant Cell* **17,** 444–463 (2005).
32. Peret, B. *et al*. *Arabidopsis* lateral root development: an emerging story. *Trends Plant Sci.* **14,** 399–408 (2009).
33. Hwang, I. & Sheen, J. Two-component circuitry in *Arabidopsis* cytokinin signal transduction. *Nature* **413,** 383–389 (2001).
34. Ruegger, M. *et al*. The TIR1 protein of *Arabidopsis* functions in auxin response and is related to human SKP2 and yeast grr1p. *Genes Dev.* **12,** 198–207 (1998).
35. Hirakawa, Y. *et al*. Non-cell-autonomous control of vascular stem cell fate by a CLE peptide/receptor system. *Proc. Natl Acad. Sci. USA* **105,** 15208–15213 (2008).
36. Mouchel, C. F., Osmont, K. S. & Hardtke, C. S. BRX mediates feedback between brassinosteroid levels and auxin signalling in root growth. *Nature* **443,** 458–461 (2006).
37. Bao, F. *et al*. Brassinosteroids interact with auxin to promote lateral root development in *Arabidopsis*. *Plant Physiol.* **134,** 1624–1631 (2004).
38. Murphy, E., Smith, S. & De Smet, I. Small signaling peptides in *Arabidopsis* development: how cells communicate over a short distance. *Plant Cell* **24,** 3198–3217 (2012).
39. Yaginuma, H., Hirakawa, Y., Kondo, Y., Ohashi-Ito, K. & Fukuda, H. A novel function of TDIF-related peptides: promotion of axillary bud formation. *Plant Cell Physiol.* **52,** 1354–1364 (2011).
40. Goda, H. *et al*. The AtGenExpress hormone and chemical treatment data set: experimental design, data evaluation, model data analysis and data access. *The Plant J.* **55,** 526–542 (2008).

METHODS

Plant materials and growth conditions. *Arabidopsis thaliana* ecotypes Col-0 and Ws-2 were used as wild-type controls and as the genetic backgrounds of the transgenic lines. The wild-type and mutant plants were grown in an environmentally controlled growth room (23 °C, 16-h light/8-h dark). *dwf12-1D, bri1, bzr1-1D* (S. Choe, Seoul National University, Korea), *pDR5–GUS* (H-T. Cho, Seoul National University, Korea), *bin2-3* (J. Chory, Salk Institute, La Jolla, USA), *pARF7–GUS* and *pARF19-GUS* (H. Fukaki, Kobe University, Japan), *tdr-1* (H. Fukuda, Tokyo University, Japan), *bin2-1, pBRI1-BRI1-GFP* (K. H. Nam, Sookmyung Women's University, Korea) and *bin2-3 bil1 bil2* (J. Li, University of Michigan, Ann Arbor, USA) were provided. *tir1-1* (CS3798), *arf7-1* (CS24607) and *arf7-1 arf19-1* (CS24625) were provided by ABRC. The *bil1* null mutant was provided by INRA (FLAG_426B01). All double and triple mutants were obtained by genetic crossing and confirmed by quantitative PCR with reverse transcription (RT–PCR) and DNA sequencing.

Quantitative RT–PCR analysis. Total RNA was isolated using Trizol reagent (Invitrogen). Double-stranded cDNA was synthesized from 1 μg RNA using oligonucleotide dT primers and ImProm-II reverse transcriptase (Promega). Quantitative real-time PCR was performed with gene-specific primers according to the instructions provided for the Light Cycler 2.0 (Roche) and the SYBR Premix Ex Taq system (Takara). To confirm T-DNA insertion knockout lines, semi-quantitative RT–PCR was performed with gene-specific primer sets (primers listed in Supplementary Table 1).

Plasmid constructs and protoplast transient expression assay. The full-length cDNAs of *BIN2*, *BIL1*, *BIL2*, *ARF7, ARF19, TIR1, TDR* and *IAA19* were cloned into plant expression vectors that contained haemagglutinin (HA) and the expression of these genes was driven by the *35S C4PPDK* promoter[31]. All point mutants of *BIN2* (*bin2-1*/*BIN2*^{E263K}, *BIN2*^{K69R}) and ARF7 (ARF7$^{S698/707A}$) were generated using the QuikChange Site-Directed Mutagenesis kit (Stratagene) according to the manufacturer's instructions. For GST-fused recombinant proteins, cDNAs of *BIN2, IAA1, IAA3, IAA14, IAA18* and *IAA19* were cloned into *pGEX 5X-1* (Promega). All cDNAs and the mutations were confirmed by DNA sequencing. For the reporter assay, 2×10^4 protoplasts were transfected with 20 μg of total plasmid DNA composed of different combinations of the reporter (*pGH3–LUC*), effectors (*ARF7–HA*, *ARF7m–HA*, *ARF19–HA*, *BIN2–HA*, *BIN2*^{E263K}*–HA*, *BIN2*^{K69R}*–HA*, *BIL1–HA, TDR–MYC* or *BIL2–HA*), and an internal control (*pUBQ10–GUS* or *p35S–Renilla*). The transfected protoplasts were then incubated at 1×10^4 cells per millilitre with or without 1 μM IAA for 3 h in the presence or absence of 1 μM TDIF. For protein expression and pulldown assays, 4×10^4 protoplasts were transfected with 40 μg of plasmid DNA composed of different combinations and incubated for 6 h at room temperature. The proteins from protoplasts were analysed by 7.5%, or 10% SDS–PAGE and visualized with anti-HA (1:2,000, Roche catalogue no. 12013819001) or anti-MYC (1:1,000, Cell Signaling catalogue no. 2276) antibody. All assays were conducted a minimum of three times and similar results were obtained in all experiments.

Physiological analysis and transgenic plants. For the analysis of LR formation, wild-type (Col-0 or Ws-2), *bin2-1*, *dwf12-1D*, *bri1*, *bri1-5, bin2-3, bil1, bil1 bin2-3, bin2-3 bil1 bil2, tdr1-1, arf7-1 bin2-1, arf7-1 arf19-1 bin2-1, tir1-1 bin2-1, bri1-5 35S–gBIN2–HA, 35S–BSU1–HA, pBES1–bes1-D–HA, pBRI1–BRI1–GFP, bzr1-1D* and *msg2-1 bin2-1* progeny of heterozygous *dwf12-1D* or *bin2-1* mutants were vertically grown on 1/2 B5 medium containing 1% sucrose and 1.2% agar type-M (Sigma) for 12 days at 23 °C with a 16-h light/8-h dark photoperiod. The number of emerged LRs and primordial cells of the seedlings were counted using differential interference contrast microscopy (Axioplan 2, Carl Zeiss) after clearing with 90% lactic acid. For auxin response assays in primary root growth or LR formation, 7-day-old Col-0, Ws-2, *bin2-1*, *dwf12-1D, bin2-3,* and *bin2-3 bil1 bil2* seedlings were transferred to 1/2 B5 media containing 0, 30 and 60 nM, or 0, 100, 500 and 1,000 nM of IAA for 4–5 days. To test the effect of bikinin (4-(5-bromopyridin-2-yl)amino-4-oxobutanoic acid) (ChemBridge Corporation) on primary root growth and LR development, seedlings were grown on 1/2 B5 media containing 5 μM bikinin for 12 days. For gene expression analysis, 5-day-old seedlings grown in MS media were transferred to MS media containing 12.5 μM bikinin for 6 h. For the TDIF response assay in LR formation, 12-day-old Col-0, *tdr1-1*, *bin2-3* and *dwf12-1D* seedlings were grown on 1/2 B5 media containing 0, 0.1, 0.5 or 1 μM TDIF with or without 5 μM bikinin. The 12-day-old Col-0, *35S–ARF7–HA* and *35S–ARF7m–HA* seedlings were grown on 1/2 B5 media containing 0, 0.5 or 1 μM TDIF. To generate transgenic plants overexpressing *ARF7–HA* or *IAA19–HA*, the coding sequences were cloned into the *pCB302ES* vector containing the 35S promoter and HA epitope tag. The constructs for *ARF7–HA, ARF7m–HA* and *IAA19–HA* were transformed into the heterozygous *dwf12-1D* and *bin2-1* mutant using the *Agrobacterium*-mediated floral dipping method, respectively. The expression levels of ARF7 or IAA19 were verified by immunoblotting with a horseradish peroxidase (HRP)-conjugated high-affinity anti-HA antibody (1:2,000, Roche catalogue no. 12013819001).

Histochemical GUS assays. Transgenic *Arabidopsis* harbouring *β-glucuronidase* (*GUS*) fused to the 3.4-kb *Arabidopsis BIN2* promoter[17], 2.0-kb *TDR* promoter or synthetic *DR5* promoter were used for histochemical GUS assays. The *pDR5–GUS / bin2-1* plant was generated by genetic crossing. For determination of *BIN2* or *TDR* expression, 7-day-old seedlings were stained with GUS-staining buffer (100 mM Tris-HCl (pH 7.0), 2 mM ferricyanide and 1 mM X-Gluc (5-bromo-4-chloro-3-indolyl-β-D-glucuronidase)) for 6 h. For determination of *pDR5–GUS* expression, seedlings were grown for 72 h on 1/2 B5 medium containing 1% sucrose, 1.2% agar type-M (Sigma) and 10 μM NPA. The seedlings were transferred to 1/2 B5 medium containing 1 μM NAA for an additional 1, 3 and 5 h, and then stained with the GUS-staining solution. For quantification of GUS activity, seedlings were homogenized with extraction buffer (150 mM sodium phosphate butter (pH 7.0), 10 mM EDTA, 10 mM β-mercaptoethanol, 0.1% Triton X-100 and 140 μM phenylmethylsulphonyl fluoride) for 5 min at room temperature. Ten microlitres of extract was incubated with 130 μl of 2 mM MUG (4-methylumbelliferyl-β-D-glucuronide) in the extraction buffer for 20 min. The reaction was terminated with 200 μl of 200 mM sodium carbonate. The fluorescence was detected with a plate reader (Perkin-Elmer) with excitation/emission at 355 nm/460 nm. For microscopic analysis of the GUS-stained seedlings, the samples were treated with 0.24 N HCl in 20% methanol for 15 min at 57 °C and replaced with 7% NaOH and 7% hydroxylamine-HCl (Sigma) in 60% ethanol for 15 min. Seedlings were dehydrated for 10 min each in 40%, 20% and 10% ethanol, and analysed by differential interference contrast microscopy (Axioplan 2, Carl Zeiss). For anatomical analysis of GUS-stained roots, stained samples were fixed for 24 h with 3% glutaraldehyde and 4% paraformaldehyde in 0.1 M phosphate buffer (pH 7.2). The fixed roots were counter-stained with 0.05% ruthenium red for 30 min and rinsed twice with 0.1 M phosphate buffer (pH 7.2). The samples were dehydrated for 1 h each in 40, 50, 60, 70, 80, 90 and 100% acetone. The specimens were infiltrated and embedded in Spurr's resin (Ted Pella) for 48 h at 65 °C using a two-step method[41]. Sections (2 μm) were cut with a MT-X ultramicrotome (RMC), mounted in 50% glycerol, and observed with a microscope (Axioplan2).

***In vivo* root confocal imaging.** DII–VENUS seedlings were grown vertically on sugar-free 1/2 MS media in 24 h light at 21 °C until 5–6 days after germination. Seedlings were transferred to 1/2 MS containing 15 μM bikinin or dimethylsulphoxide as a control and incubated overnight. Seedlings were mounted on glass slides and imaged using a Leica SP5 confocal microscope (Leica; a 514 nm detector using gain value 100%, offset value 28.98, averaged over 4 frames). Static images were taken of root tips and mature sections of primary root for each treatment. Fluorescence was quantified as the raw integrated density value, measured using FIJI software[42].

Protein–protein interaction, immunoblotting and *in vitro* kinase assays. For interaction between BIN2 and TDR kd (TDR kinase domain) in yeast cells, the yeast strain AH109 was transformed with *pGBKT7–BIN2* and *pGADT7–TDR*-kd by the LiAc method. Transformed yeasts were grown on synthetic medium lacking Leu, Trp and His containing 3 mM 3-aminotriazole or medium lacking Leu and Trp. For purification of GST-fused recombinant proteins, *GST–BIN2, GST–IAA1, GST–IAA3, GST–IAA14, GST–IAA18, GST–IAA19* or *d2-ARF7* (encoding the QSL-rich C-terminal domain of ARF7) were expressed in *Escherichia coli* BL21. Bacterial cells were grown in 200 ml of Luria broth medium at 37 °C until $D_{600\,nm} = 0.8$ and further incubated with 0.5 mM IPTG (isopropyl β-D-1-thiogalactopyranoide) for 3 h. The recombinant GST-tagged proteins were purified according to the manufacturer's protocol (GE Healthcare). For pulldown assays, HA-tagged *ARF7, TDR* or *ARF19* was transfected into protoplasts. Protoplasts were then incubated for 6 h to permit transgene expression. The transfected protoplasts were lysed using immunoprecipitation buffer (50 mM Tris-HCl (pH 7.5), 75 mM NaCl, 5 mM EDTA, 1 mM dithiothreitol, 1 × protease inhibitor cocktail (Roche) and 1% Triton X-100). Total protoplast lysates were incubated with 1 μg of recombinant GST or GST–BIN2 proteins for 1 h. To determine the binding affinities between phosphorylated ARF7 and AUX/IAAs, *ARF7–HA* was co-transfected with or without either *BIN2–HA* or *BIN2* ^{K69R}*–HA* into protoplasts. After 6 h of incubation, total lysates from the transfected protoplasts were incubated with 1 μg of GST or 100 ng GST–IAA1, GST–IAA3, GST–IAA14, GST–IAA18 or GST–IAA19 for 1 h in the presence of 10 μM MG132. For monitoring TIR1/ARF7/IAA19 triple complex formation, *ARF7–HA* and *TIR1–HA* were co-transfected into protoplasts with or without *BIN2–HA*. Protoplast lysates were incubated with 1 μg of GST or 100 ng of GST–IAA19 for 1 h in the presence of 10 μM MG132. The lysates were then precipitated with glutathione Sepharose 4B. The precipitated proteins were detected using a HRP-conjugated high-affinity anti-HA antibody. Calf intestine alkaline phosphatase treatment was performed in immunoprecipitation buffer for 20 min

DOI: 10.1038/ncb2893

at 37 °C. For immunoblotting analyses, 3–20 μg of proteins from protoplasts or seedlings was analysed by 7.5% (or 10%) SDS–PAGE and visualized with HRP-conjugated high-affinity anti-HA antibody. For determination of IAA19 protein half-life, wild-type (Col-0) and *bin2-1* homozygote plants expressing *35S–IAA19–HA* were grown in 1/2 B5 media containing dimethylsulphoxide or 5 μM bikinin, and incubated for the indicated times with 100 μM cycloheximide. The proteins from seedlings were analysed by 10% SDS–PAGE and visualized with anti-HA or anti-actin (1:1,000, MP biomedical catalogue no. 69100) antibody. The half-life was calculated by a regression analysis[43]. For the *in vitro* kinase assay, typically, 10 μg of GST–ARF7 QSL-rich C-terminal domain was incubated with or without 5 μg of GST–BIN2 in a kinase buffer (20 mM Tris-HCl (pH 7.5), 100 mM NaCl, 12 mM $MgCl_2$, 100 μM ATP and 10 μCi of [γ-^{32}P]ATP). After incubation for 2 h at 37 °C, the proteins were subjected to 10% SDS–PAGE and the phosphorylated proteins were visualized by autoradiography.

Chromatin immunoprecipitation. Two-week-old *35S–ARF7–GFP/arf7-1* seedlings (5 g) were treated with 1 μM NAA and 50 μM bikinin for 4 h. Two-week-old *35S–ARF7–HA* and *35S–ARF7–HA/dwf12-1D* (5 g) were also used for ChIP assay. ChIP assays for ARF19 were performed with Col-0 or *bin2-1-gof* using anti-ARF19 antibody after 2 h of 1 μM 2.4D treatment with or without 50 μM bikinin. The seedlings were crosslinked with 1% formaldehyde for 10 min and quenched with 125 mM glycine. The ground tissues were resuspended with nuclei isolation buffer (0.25 M sucrose, 15 mM PIPES (pH 6.8), 5 mM $MgCl_2$, 60 mM KCl, 15 mM NaCl, 1 mM $CaCl_2$, 1% Triton X-100 and 1 mM phenylmethylsulphonyl fluoride) for 30 min at 4 °C. The nuclear pellets were resuspended in nuclei lysis buffer (50 mM HEPES (pH 7.0), 150 mM NaCl, 1 mM EDTA, 1% SDS, 1% Triton X-100, 1 mM phenylmethylsulphonyl fluoride and 1 X Protease inhibitor cocktail for plant cell and tissue extracts (Sigma)) and sonicated to produce ~0.5–1 kb DNA fragments. After sonication, chromatin fractions were diluted tenfold with nuclei lysis buffer and pre-cleared with protein G agarose/salmon sperm DNA (Millipore) for 1 h at 4 °C. The protein–DNA complexes were immunoprecipitated with anti-GFP antibody (1:1,000, Santa-Cruz Biotech catalogue no. sc-8334), anti-HA antibody (1:1,000, Abcam catalogue no. ab9110) or 1–3 μg of anti-ARF19 antibody (1:1,000, home-generated) overnight at 4 °C and further incubated with protein G agarose/salmon sperm DNA for 1 h at 4 °C. After washing with low salt buffer (150 mM NaCl, 20 mM Tris-HCl (pH 8.0), 0.2% SDS, 0.5% Triton X-100 and 2 mM EDTA) for 5 min at 4 °C and high-salt buffer (500 mM NaCl, 20 mM Tris-HCl (pH 8.0), 0.2% SDS, 0.5% Triton X-100 and 2 mM EDTA) for 5 min at 4 °C, the immunocomplexes were eluted twice by elution buffer (0.5% SDS and 0.1 M $NaHCO_3$) and then reverse crosslinked with 200 mM NaCl for 6 h at 65 °C. After removing proteins with proteinase K, DNAs were purified by phenol–chloroform extraction and recovered by ethanol precipitation. Precipitated DNAs were resuspended with TE buffer (10 mM Tris-HCl (pH 8.0) and 1 mM EDTA) and used as PCR templates (primers listed in Supplementary Table 1).

Identification of phosphorylation sites. Recombinant GST–tARF7 proteins phosphorylated by GST–BIN2 for 12 h *in vitro* were subjected to in-solution digestion. The proteins were resolved in a digestion solution (6 M urea and 40 mM ammonium bicarbonate dissolved in HPLC-grade water). Protein reduction was performed with 5 mM dithiothreitol for 30 min, followed by an alkylation step with 25 mM iodoacetamide in the dark for 30 min at room temperature. The sample was digested with sequencing-grade modified trypsin (Promega) overnight at 37 °C. The digested proteins were collected and desalted with the C-18 spin column (Thermo). Phosphopeptides were enriched with the SwellGel gallium-chelated disc (Pierce) according to the manufacturer's instructions. Phosphopeptides were analysed on a linear ion trap LTQ XL mass spectrometer (Thermo) interfaced with a nano-electrospray ion source. Chromatographic separation of peptides was achieved using a NanoLC• 2D system (Eksigent), equipped with a capillary column (a 10 cm PicoTip emitter, 75 μm inner diameter) packed in-house with Magic C18AQ 5 μ 200 Å particles (Michrom BioResources). Peptides mixtures were loaded from an Eksigent auto sampler and separated using a linear gradient of ACN/water (2–40% ACN in 40 min), containing 0.1% formic acid, at a flow rate of 260 nl min^{-1}. A full MS scan was performed in the range of 300–2,000 m/z, and a data-dependent MS/MS (MS^2) scan on the four most intense precursor ions. The MS/MS spectra were searched against the TAIR 10 protein sequence database using SEQUEST algorithm in the Proteome Discoverer software (Thermo) with the following parameters: semi-trypsin, a mass tolerance of 2.0 and 1.0 Da for precursor and fragment ions, respectively, carbamidomethylation of cysteine (+57.021) as a fixed modification, and oxidation of methionine (+15.995) and phosphorylation of serine, threonine and tyrosine (+79.966) as variable modifications. The phosphorylated peptides were identified using XCorr cutoff scores of 1.5, 2.0 and 2.5 for singly, doubly and triply charged peptides, respectively. All phosphorylation sites were confirmed by manual interpretation.

Statistical analysis. Statistical analysis was performed using Student's t-test with a two-tailed distribution. No statistical method was used to predetermine sample sizes. No samples have been excluded. The experiments were not randomized. The investigators were not blinded to allocation during experiments and outcome assessment. To determine the appropriate statistical tests, the data were tested for normal distribution.

41. De Smet, I. *et al.* An easy and versatile embedding method for transverse sections. *J. Microsc.* **213,** 76–80 (2004).
42. Schindelin, J. *et al.* Fiji: an open-source platform for biological-image analysis. *Nat. Methods* **9,** 676–682 (2012).
43. Chang, C. S., Maloof, J. N. & Wu, S. H. COP1-mediated degradation of BBX22/LZF1 optimizes seedling development in *Arabidopsis*. *Plant Physiol.* **156,** 228–239 (2011).

DOI: 10.1038/ncb2893

nature cell biology

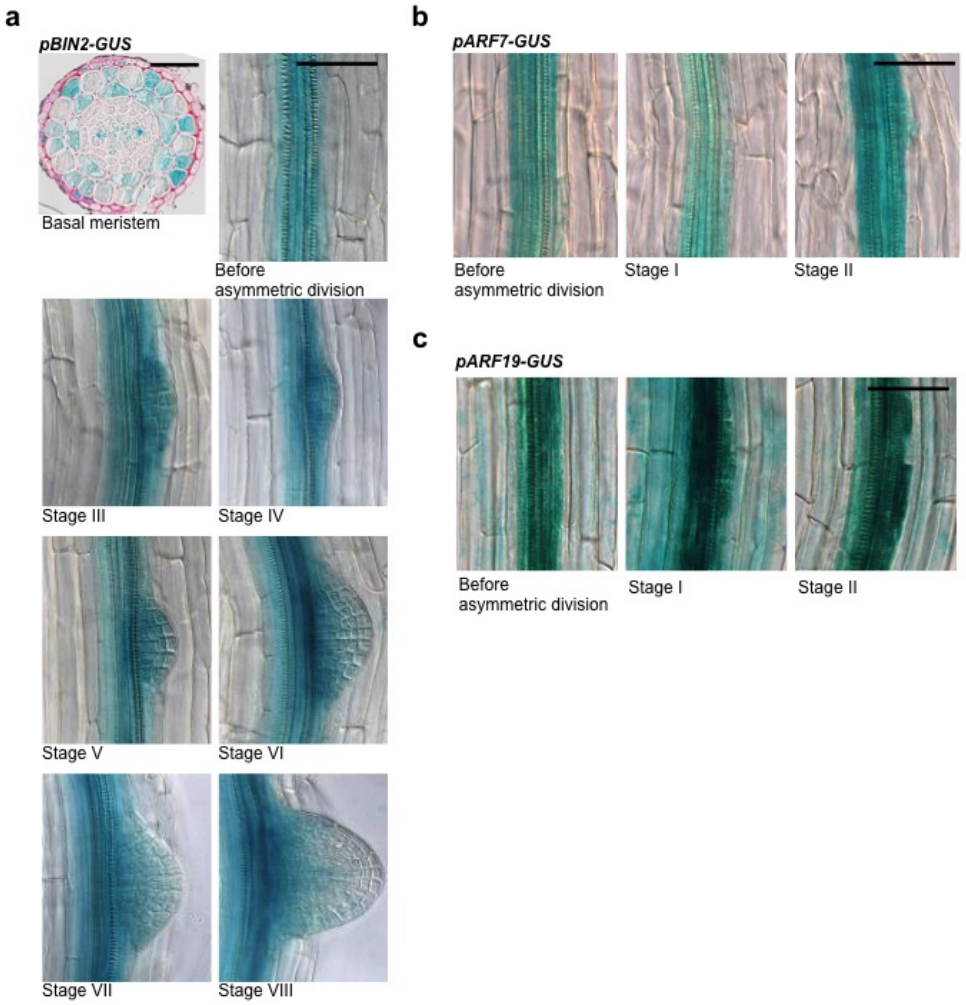

Supplementary Figure 1 The expression pattern of *BIN2, ARF7* and *ARF19* in root. (**a**) *BIN2* expression in basal meristem and LRP at different stages of lateral root development. Note that the expression is restricted to the basal part of LRP at stages IV-VII. Scale bar, 50 μm. (**b, c**) *ARF7* (**b**) and *ARF19* (**c**) expression in LRP at early stages of lateral root development. GUS activity driven by the *ARF7* or *ARF19* promoter was observed in early stages of LRP. Scale bar, 50 μm.

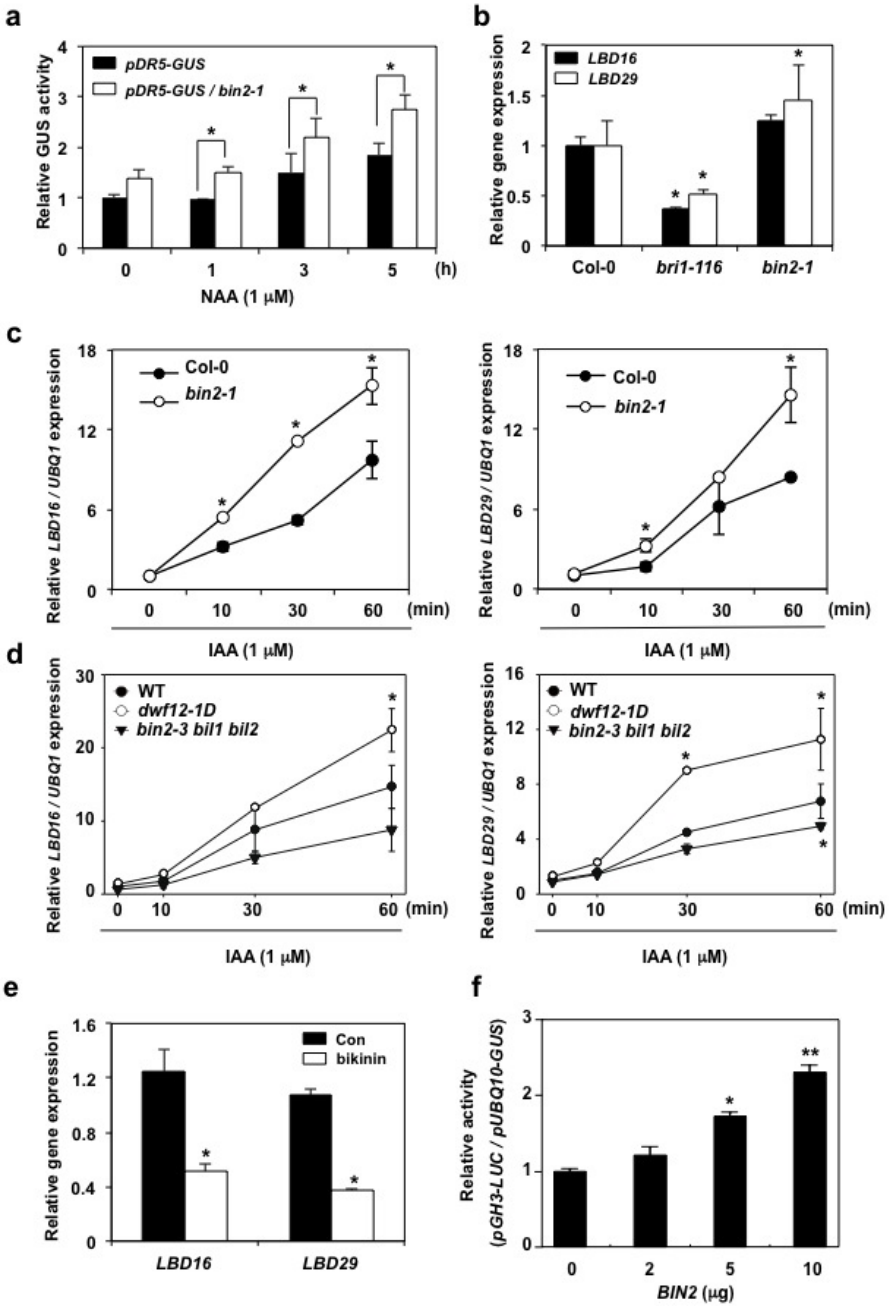

Supplementary Figure 2 BIN2 enhances auxin-response in plants. (**a**) Three-day-old seedlings of *pDR5-GUS* and *pDR5-GUS / bin2-1-gof* grown on 10 μM NPA-containing medium were transferred to 1 μM NAA-containing medium, and further treated for 1, 3, and 5 h. The GUS activity of the seedlings was measured. Error bars indicate SEM (n=3, 20 plants per n=1, * for p<0.05 by student's t-test). (**b**) The expression levels of *LBD16* and *LBD29* in 10-day-old *bri1-116* and *bin2-1-gof* (+/+) mutants were determined by quantitative RT-PCR (n=4, 10 plants per n=1, * for p<0.05 by student's t-tests). (**c, d**) The expression levels of *LBD16* (left panel) and *LBD29* (right panel) in 10-day-old WT and *bin2-1-gof* (**c**), *dwf12-1D-gof* (**d**), and *bin2-3 bil1 bil2* mutants were determined by quantitative RT-PCR after auxin treatment for the indicated times. Error bars indicate SEM (n=3, 10 plants per n=1, * for p<0.05 by student's t-tests). (**e**) Bikinin treatment represses *LBD16* and *LBD29* expression. Error bars indicate SEM (n=3, 10 plants per n=1, * for p<0.05 by student's t-tests). (**f**) BIN2 enhances the activity of *pGH3-LUC* auxin-responsive reporter in a dose-dependent manner. Protoplasts were co-transfected with *pGH3-LUC*, indicated amount of *BIN2-HA,* and *pUBQ10-GUS* (internal control). Error bars indicate the SEM (n = 4, 20,000 cells per n=1, * for p<0.05, ** for p<0.01 by student's t-test). Statistics source data found in Supplementary Table 2. Details on the statistical analysis are found in Methods.

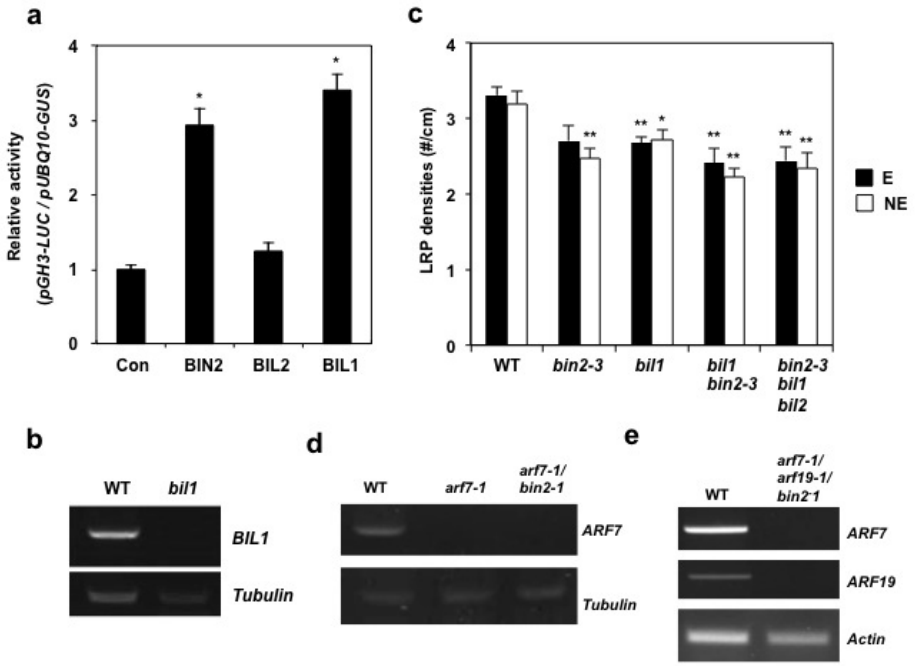

Supplementary Figure 3 BIN2 and BIL1 are involved in lateral root formation. (**a**) BIN2 and BIL1 enhance auxin-responsive *pGH3-LUC* activity. Protoplasts were cotransfected with *pUBQ10-GUS* (internal control), *pGH3-LUC* and an effector plasmid harboring *BIN2, BIL1* or *BIL2*. Error bars indicate SEM (n = 4, 20,000 cells per n=1, * for p<0.05 by student's t-test). (**b**) Isolation of *bil1* knockout mutant. The transcripts of *BIL1* in 7-day-old wild type (Ws-2) and *bil1* (FLAG_426B01) were determined by semi-quantitative PCR. (**c**) Lateral root densities of twelve-day-old seedlings of WT (Ws-2), *bin2-3-lof*, *bil1*, *bil1 bin2-3* and *bin2-3 bil1 bil2* mutant. E, emerged lateral roots; NE, non-emerged LRP. Error bars indicate SEM (n=15 plants, * for p<0.05, ** for p<0.01 by student's t-test). (**d**) The transcripts of *ARF7* in WT (Col-0), *arf7-1* and *arf7-1 bin2-1-gof* were determined by semi-quantitative PCR. (**e**) The transcripts of *ARF7* and *ARF19* in WT (Col-0) and *arf7-1 arf19-1 bin2-1-gof* were determined by semi-quantitative PCR. *Tubulin* and *Actin2* genes served as input controls. Details on the statistical analysis are found in Methods.

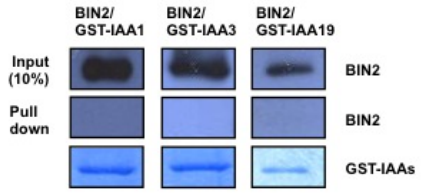

Supplementary Figure 4 BIN2 does not interact with AUX/IAA proteins. HA-tagged *BIN2* was expressed in protoplasts. Protoplast lysates were incubated with GST-IAA1, GST-IAA3, or GST-IAA19 proteins for 1 h, and then precipitated with glutathione sepharose 4B. BIN2 proteins were detected with anti-HA antibody (upper and middle panels), and GST-tagged IAA1, IAA3, or IAA19 proteins were visualized by Coomassie blue staining (lower panel).

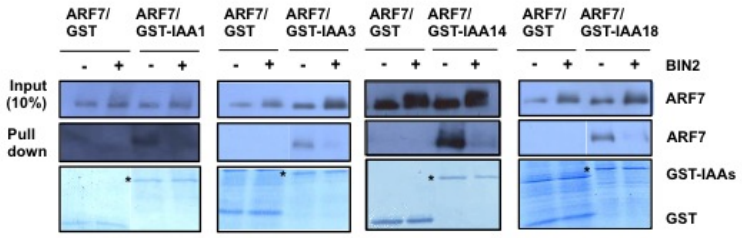

Supplementary Figure 5 BIN2-mediated phosphorylation of ARF7 attenuates its interaction with IAA1, IAA3, IAA14 and IAA18. Protoplast lysates overexpressing *ARF7-HA* or *ARF7-HA* and *BIN2-HA* were incubated with purified GST-tagged IAA1, IAA3, IAA14, or IAA18 proteins and pulled down with glutathione sepharose 4B. The pulled-down proteins were analyzed with anti-HA antibody. The GST protein was used as a negative control. An asterisk indicates GST-IAAs proteins.

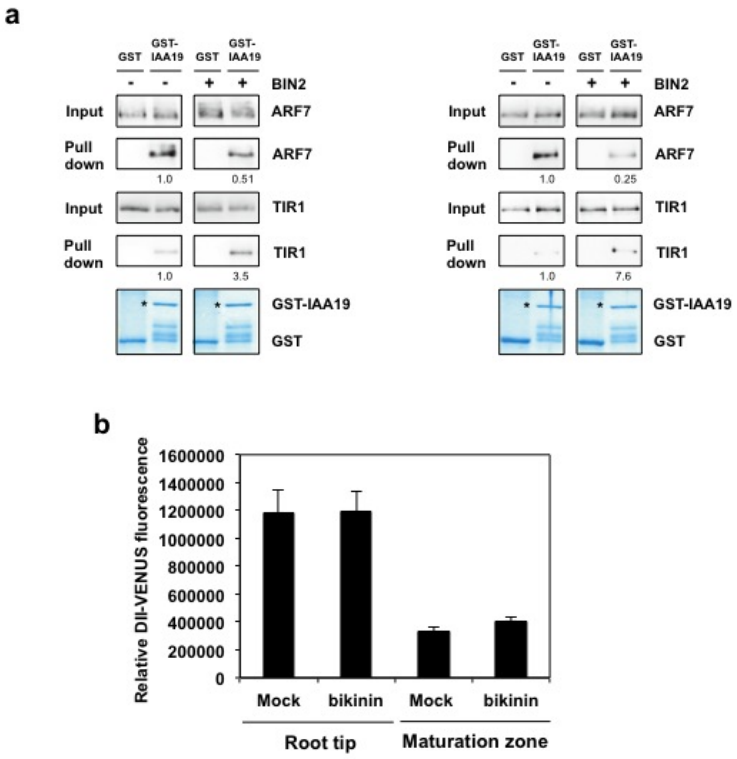

Supplementary Figure 6 (**a**) BIN2-mediated phosphorylation of ARF7 results in increased binding of IAA19 with TIR1. Two more independent pull down experiments conducted in Fig. 6a are presented. HA-tagged *ARF7* and *TIR1* were co-transfected into protoplasts with or without *BIN2-HA*. After 6 h of incubation, protoplast lysates were incubated with purified GST-IAA19 proteins and 10 μM of MG132 for 1 h, and then pulled down with glutathione sepharose 4B. GST-IAA19-bound proteins were visualized with anti-HA antibody. GST protein was included as a negative control. Asterisks indicate GST-IAA19 proteins. The levels of GST-IAA19 pulled-down proteins were normalized to those of the input proteins. The normalized intensities of the pulled-down proteins in the absence of BIN2 were set to 1, and the relative protein intensities were presented under the corresponding protein bands. (**b**) Relative DII-VENUS intensities in seedlings of mock or 15 μM bikinin treated WT (Col-0). (n=20 plants).

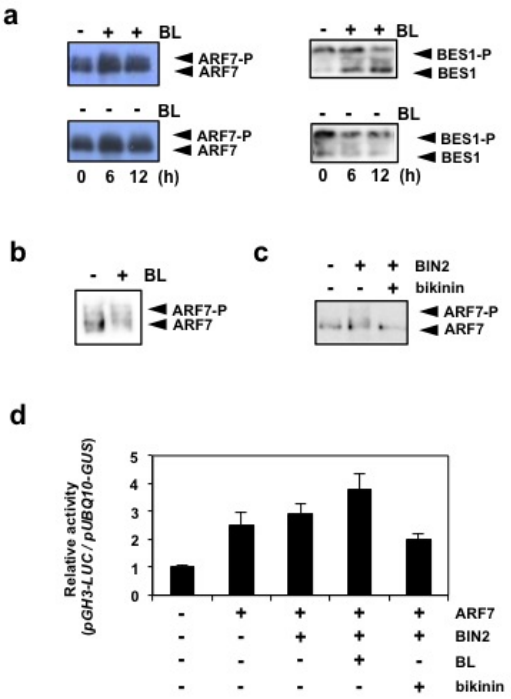

Supplementary Figure 7 Brassinosteroid is not involved in BIN2-mediated ARF7 activation. (**a, b**) Brassinosteroid does not affect the phosphorylation status of ARF7. Seven-day-old transgenic seedlings harboring *35S-ARF7-HA* (left panel), *35S-ARF7-HA / dwf12-1D-gof* (**b**), or *35S-BES1-HA* (a positive BR-responsive control, right panel) were incubated with or without 20 nM of epi-BL for 6 and 12 h. The phosphorylation status of HA-tagged ARF7 and BES1 was determined as the protein mobility shift with anti-HA antibody. (**c**) Bikinin inhibits BIN2-induced phosphorylation of ARF7. *ARF7-HA* was co-transfected with *BIN2-HA* into protoplasts and incubated with or without 30 μM of bikinin for 6 h. ARF7 proteins were visualized with anti-HA antibody. (**d**) Brassinosteroid could not suppress the BIN2 actions for enhancing the transcriptional activity of ARF7. *ARF7-HA, pGH3-LUC* and *pUBQ10-GUS* were cotransfected into protoplasts with or without *BIN2-HA.* The protoplasts were incubated with or without 1 μM epi-BL and 30 μM bikinin for 6 h. Error bars indicate SEM (n=4, 20,000 cells per n=1).

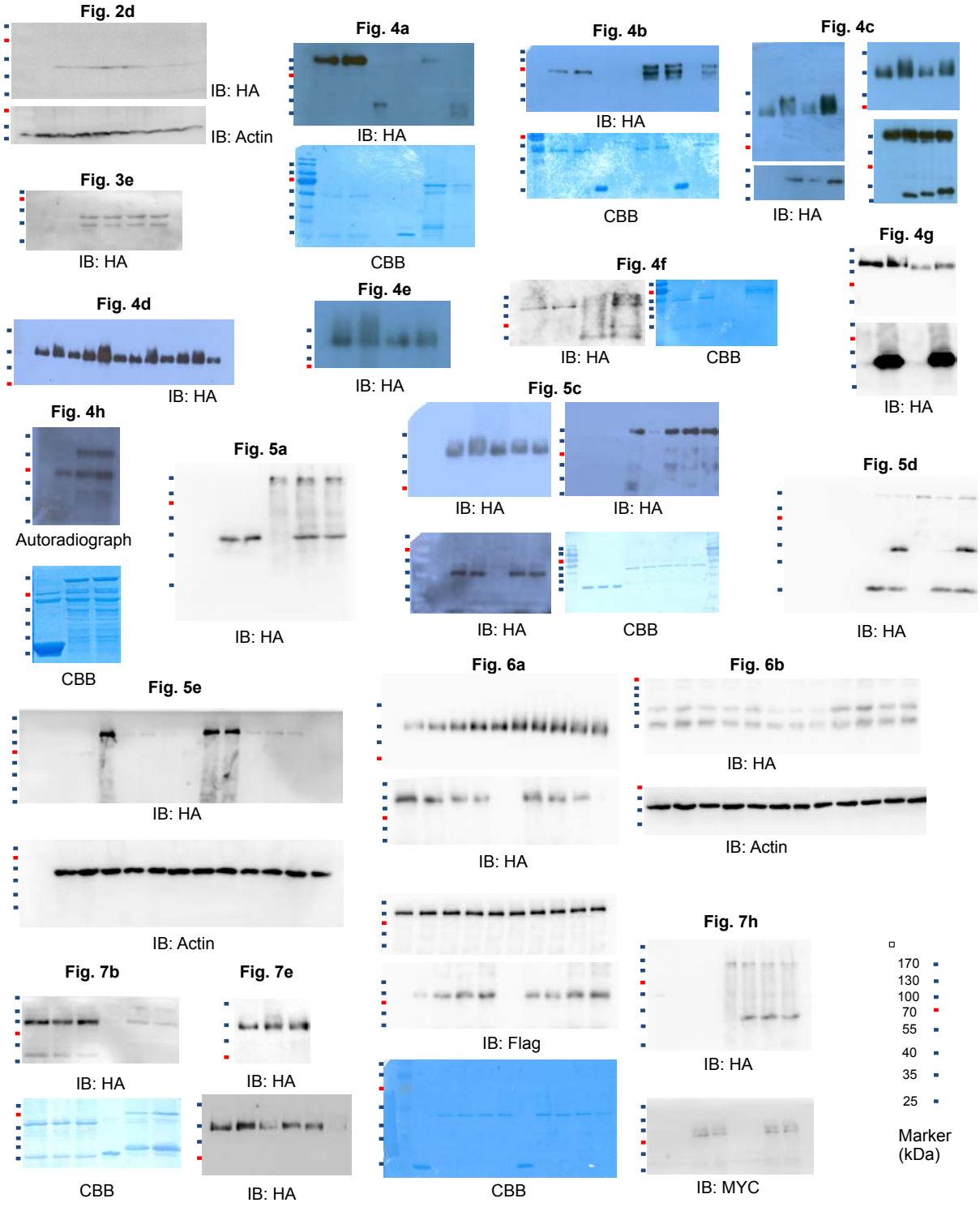

Supplementary Figure 8 Full scan data of immunoblot and in vitro kinase assay

Supplementary Table Legends

Supplementary Table 1 Primer combinations for quantitative PCR

Supplementary Table 2 Statistics source data